

The magnetic structure of the Jahn-Teller system LaTiO_3

Robert Schmitz,¹ Ora Entin-Wohlman,² Amnon Aharony,² A. Brooks Harris,³ and Erwin Müller-Hartmann¹

¹*Institut für Theoretische Physik, Universität zu Köln, Zùlpicher Straße 77, 50937 Köln, Germany*

²*School of Physics and Astronomy, Raymond and Beverly Sackler Faculty of Exact Sciences,
Tel Aviv University, Tel Aviv 69978, Israel*

³*Department of Physics and Astronomy, University of Pennsylvania, Philadelphia, Pennsylvania 19104, USA*
(March 22, 2022)

We investigate the effect of the experimentally observed Jahn-Teller distortion of the oxygen octahedra in LaTiO_3 on the magnetic exchange. We present a localized model for the effective hopping between nearest-neighbor Ti ions and the intra-site Coulomb interactions, based on a non-degenerate orbital ground state due to the static crystal field. The latter corresponds to an orbital order which recently has been confirmed experimentally. Using perturbation theory we calculate, in addition to the Heisenberg coupling, antisymmetric and symmetric anisotropy terms of the superexchange spin Hamiltonian which are caused by the spin-orbit interaction. Employing our superexchange Hamiltonian, we deduce the magnetic order at low temperatures which is found to be in good agreement with experiment.

PACS numbers: 71.10.-w, 71.27.+a, 71.70.Ch, 75.10.Dg, 75.25.+z, 75.30.Et

I. INTRODUCTION

In the seventies, the orthorhombic perovskite LaTiO_3 was considered as a typical example of an antiferromagnetic Mott insulator ($T_N = 146 \text{ K}$).¹ The ground state of the Ti ion is trivalent with a single electron in the d shell. Recently, LaTiO_3 has attracted attention when an ordered magnetic moment of $0.46 \mu_B$ was reported.² This value is surprisingly small for a single electron with quenched orbital moment, for which one would have expected $1 \mu_B$. In LaTiO_3 , this value may be reduced by about 17% due to quantum fluctuations of the 3D Heisenberg model, and by about further 14% due to the on-site spin-orbit coupling, (in conjunction with the crystal field, see below), leading to an overall estimate of $0.72 \mu_B$.

A previous attempt to explain this unexpected finding has neglected the Jahn-Teller distortion of the oxygen octahedra in LaTiO_3 and assumed that the symmetry of the unit cell is strictly cubic. In such a situation the t_{2g} ground state of the Ti ion is three-fold degenerate and the orbital moment is unquenched. Hence, it was proposed to consider LaTiO_3 as an orbital liquid in order to explain the reduction of the ordered moment by orbital fluctuations.³

However, recent experiments give a strong indication of the importance of the Jahn-Teller distortion in LaTiO_3 , and in particular enable, using recent structural data, to estimate the splitting it induces in the t_{2g} levels: There is a crystal-field gap of about 0.2 eV between the non-degenerate ground state and the next excited level.⁴ This value has been confirmed by a study of photoelectron spectroscopy⁵ and is at least one order of magnitude higher than any superexchange energy in LaTiO_3 .⁶ Consequently, the orbital order at low temperatures is not induced by the superexchange. Rather, the orbital degree of freedom is frozen by the crystal field. The scenario of

suppressed orbital fluctuations has also been confirmed by a recent LDA+DMFT study.⁷ The assumption of Ref. 8 that the crystal-field splitting, the superexchange, and the spin-orbit coupling are all of the same order is inconsistent with the photoelectron spectroscopy of Ref. 5. In addition, a higher value, $0.57 \mu_B$, of the ordered moment has been recently reported,⁴ making the discrepancy between experiment and theory (which gives $0.72 \mu_B$) even smaller.

The Jahn-Teller effect in LaTiO_3 is caused by the twisting of the Ti–O bonds with respect to each other (i.e. by differences between the O–O bond lengths), rather than by differences between the Ti–O bond lengths. The non-degenerate ground-state orbital due to crystal-field calculations given in Ref. 4 is consistent with the orbital order found in NMR measurements of the Ti– $3d$ quadrupole moment.⁹ The presence of orbital order at low temperatures has been also concluded from measurements of the dielectric properties and the dynamical conductivity.¹⁰ As opposed to these findings, an orbital contribution to the specific heat, which is predicted by the orbital-liquid model, has not been found in experiment.¹¹

Hence, from the recent experiments it must be concluded that the orbital-liquid model is inappropriate for LaTiO_3 . Moreover, it has been proven, by exact symmetry arguments, that due to a hidden symmetry the superexchange Hamiltonian used in Ref. 3 cannot reproduce the observed magnetic order of LaTiO_3 .^{12,13}

Another model to explain the magnetic properties of LaTiO_3 proposed the lifting of the t_{2g} degeneracy by the crystal field resulting from the eight La ions which surround each TiO_6 octahedron—assuming undistorted octahedra, i.e. neglecting the Jahn-Teller effect.¹⁴ This model predicts a realistic non-degenerate ground-state orbital for each Ti ion,^{6,9} and yields plausible values for the Heisenberg couplings between nearest-neighbor Ti

ions.

However, there are two points missing in the calculations of Ref. 14. (i) The crystal field due to the eight nearest La ions, which gives a nearly equidistant splitting scheme between the three t_{2g} orbitals, is only a first approximation of the full crystal field due to all ions of the solid. It is preferable to treat the electrostatic crystal field more accurately, employing the Madelung sum. Such a treatment shows that the Jahn-Teller effect leads to a non-degenerate t_{2g} ground-state orbital and two quasi-degenerate excited orbitals.⁴ (ii) Terms of the exchange Hamiltonian which break the spin-rotational invariance and cause the magnetic order have not been considered. Hence, the origin of the observed magnetic order is not fully understood so far.

In the present paper, we investigate a model for the magnetism of LaTiO_3 , which starts from a point-charge calculation of the static crystal field for the Ti ions via a full Madelung sum over the crystal (as was already discussed in Ref. 4). Taking into account the recent structural low-temperature data and using a Slater-Koster parametrization of the Ti-O hopping, we calculate an effective hopping matrix between the d orbitals of nearest-neighbor Ti ions. Treating this Ti-Ti hopping and the on-site spin-orbit coupling as perturbations, we calculate the superexchange coupling between the non-degenerate crystal-field ground states of the Ti^{3+} ions. In treating the Ti^{2+} ions, which appear as intermediate states of the exchange processes, we take into account the full on-site Coulomb correlations in terms of Slater integrals and diagonalize the Coulomb Hamiltonian together with the crystal-field one. The spin-orbit coupling gives rise to antisymmetric and symmetric anisotropies of the spin Hamiltonian. We calculate the isotropic part of the exchange coupling and both kinds of the anisotropies to leading orders. Using our exchange Hamiltonian, we determine the classical ground state which gives the directions of the spins in the ordered phase. The experimental data reveals a G-type antiferromagnetic order along the crystallographic a axis, which is accompanied by a small ferromagnetic moment along the c axis.⁴ Our calculation reproduces this order. In addition, we find a small A-type moment along the b axis, which has not yet been detected experimentally.

In the next section we present the details of our model. Section III is devoted to the perturbation expansion yielding the microscopic spin Hamiltonian. Section IV discusses the macroscopic magnetic Hamiltonian and the resulting magnetic order of the classical ground state. It includes as well a detailed comparison with existing experimental data. Finally, we summarize our results in Sec. V.

II. THE MODEL

A. The crystal field

The unit cell of LaTiO_3 contains four Ti ions, see Fig. 1 and Table I (the Tables are given on pages 18ff.), and has the symmetry of the space group $Pbnm$ (No. 62 in Ref. 15). The symmetries of this space group are listed in Table II. Given the position of one La, Ti, O1, and O2 ion each (see Table I), the positions of all other ions in the unit cell follow from the space-group symmetries. In order to use these symmetries conveniently, we employ in our calculation the orthorhombic orthonormal¹⁶ basis for the Ti- d orbitals

$$|xy\rangle, |2z^2\rangle, |yz\rangle, |xz\rangle, |x^2 - y^2\rangle, \quad (1)$$

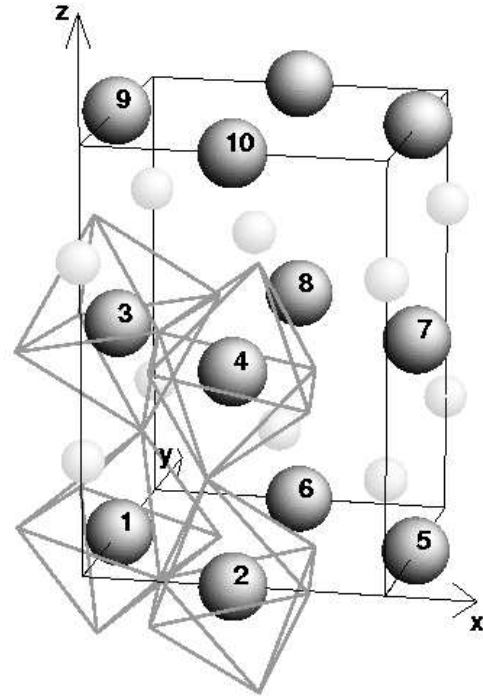


FIG. 1. The crystallographic structure of LaTiO_3 . The ten Ti ions, which constitute the twelve inequivalent nearest-neighbor Ti-Ti bonds are enumerated. For simplicity, oxygen octahedra are only shown around the four crystallographically inequivalent Ti sites. La ions from two layers are shown as small spheres. For example, the sites 2 and 6 are crystallographically equivalent but the bond 61 emerges from the 12 bond by a glide reflection, so that the effective hopping matrix for the bond 16 is different than that of the 12-bond: It is the transposed one, see Table IV.

where the x, y and z axes correspond to the crystallographic a, b and c axes. In a cubic perovskite, the first two orbitals would correspond to the e_g orbitals and the three others to the t_{2g} orbitals. [Note that the pseudocubic basis for the d orbitals, which is frequently used, is

obtained from Eq. (1) upon rotating the x and y axes by 45° around the z direction.]

Using the structural data of Ref. 4 (taken at $T = 8$ K), we have calculated the spectrum and the eigenstates for the Ti ion located at $(0, 1/2, 0)$, employing a point-charge calculation of the static crystal-field Hamiltonian. This calculation uses the full Madelung sum over the crystal (which is evaluated as an Ewald sum, see Appendix A). It requires the second moment, $\langle r^2 \rangle$, and the fourth moment, $\langle r^4 \rangle$, of the effective ionic radius of the Ti^{3+} -ion, see Appendix A. We have used the values $\langle r^2 \rangle = 0.530 \text{ \AA}^2$ and $\langle r^4 \rangle = 0.554 \text{ \AA}^4$.¹⁷ The results of the crystal-field calculation, which are listed in Table III, exhibit a typical Jahn-Teller t_{2g} splitting scheme, where a non-degenerate ground state is clearly separated from the two quasi-degenerate excited states.

The orbital order due to the static crystal field is shown in Fig. 2. The ground-state orbital is given by

$$|0\rangle = 0.770|yz\rangle \pm 0.636|x^2 - y^2\rangle. \quad (2)$$

This state has approximately the $2z^2$ structure in the coordinate system in which the y and z axes are rotated by $\pm 56^\circ$ around the x axis.⁴ The relative sign of the linear combination alternates between neighboring ab planes according to the mirror planes at $z = 1/4$, etc. In the pseudo-spin language,¹⁸ we have ferro-orbital order in the ab planes and canted antiferro-orbital order between the planes. We note that this ground state is in perfect agreement with experiment.⁹ The ground state cited in Refs. 9 and 14 is given, to a good approximation, by

$$|0'\rangle = \underbrace{\sqrt{\frac{2}{3}}}_{0.816} |yz\rangle \pm \underbrace{\frac{1}{\sqrt{3}}}_{0.577} |x^2 - y^2\rangle. \quad (3)$$

It practically coincides with our ground state,

$$|\langle 0|0'\rangle|^2 = 99.06\%. \quad (4)$$

The ground state $|0\rangle$ [see Eq. (2)] of the crystal field, which is occupied at each Ti site by a single electron, is the starting point of our model. The perturbative calculation outlined below is employed in order to evaluate the magnetic superexchange coupling between Ti ions in this state.

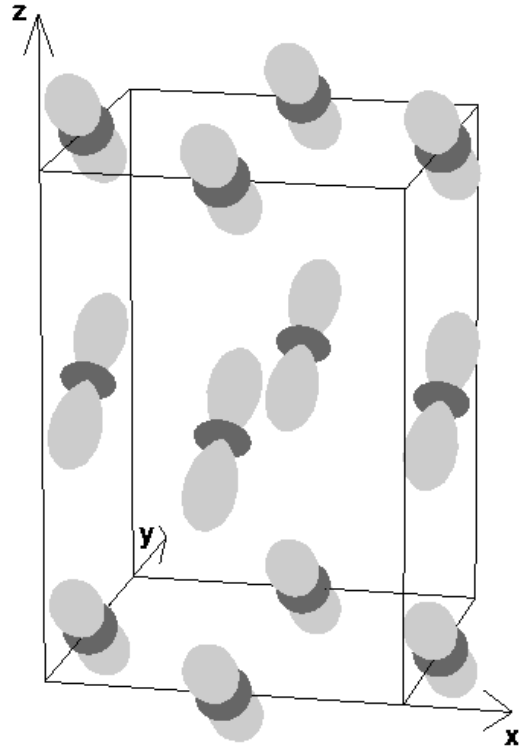


FIG. 2. The orbital order of the Ti ions resulting from the calculated crystal field (the energy scale of the superexchange which could in principle also affect the orbital degree of freedom is about one order of magnitude smaller than the crystal-field gap). The order is ferro-orbital in the ab planes and canted antiferro-orbital between the planes.

B. The Hamiltonian

The perturbation scheme is applied to a two-site cluster consisting of two nearest-neighbor Ti ions, denoted by m and n . The unperturbed Hamiltonian acting on such a cluster is given by

$$H_{mn}^0 = H_{mn}^{\text{cf}} + H_{mn}^{\text{c}}, \quad (5)$$

where H_{mn}^{cf} is the static crystal field and H_{mn}^{c} describes the intra-ionic Coulomb correlations of a doubly occupied d shell. The perturbation calculation requires a selected set of eigenstates and the corresponding eigenenergies of H_{mn}^0 . In our case, the eigenstates span a Hilbert space which consists of two sectors. In the first, termed the Ti^{3+} sector, both Ti ions are trivalent. In the second, called the Ti^{2+} sector, one of the Ti ions is divalent (two d electrons on the same site) and the other is four-valent (an empty d shell). In the ground state of H_{mn}^0 , which belongs to the Ti^{3+} sector, both Ti ions are in the one-particle ground state of H_{mn}^{cf} , modulo spin up or down on each site. This leads to a four-fold degeneracy of the ground state of the cluster. The complete Ti^{3+} sector has 100 basis states (made up of five orbital and two

spin states on each of the two sites). The Ti^{2+} sector has 90 basis states (30 spin-triplet states and 15 spin-singlet states of the doubly occupied d shell and a factor of 2 because each of the Ti ions can be doubly occupied while the other has an empty d shell).

In order to calculate the spectrum of H_{mn}^0 , we apply H_{mn}^{cf} on the Ti^{3+} sector, and both H_{mn}^{cf} and H_{mn}^{c} on the Ti^{2+} sector. H_{mn}^{c} is parametrized in terms of the Slater integrals F_2 and F_4 ,¹⁹ and the effective Ti–Ti charge-transfer energy U_{eff} . This energy is the difference between the four-fold degenerate ground state of the cluster (which is the lowest level of the Ti^{3+} sector) and the lowest level of the Ti^{2+} sector (where H_{mn}^{cf} and H_{mn}^{c} are diagonalized simultaneously). We use $F_2 = 8F_4/5 = 8.3 \text{ eV}$ from an atomic Hartree-Fock calculation,²⁰ and $U_{\text{eff}} = 3.5 \text{ eV}$ from the analysis of the photoemission spectra and first-principles calculations.²¹

The perturbation part of the Hamiltonian, V_{mn} , consists of an effective Ti–Ti tunnelling term, H_{mn}^{tun} , and the on-site spin-orbit interaction, H_{mn}^{so} ,

$$V_{mn} = H_{mn}^{\text{tun}} + H_{mn}^{\text{so}}. \quad (6)$$

The tunnelling Hamiltonian is given in terms of an effective hopping matrix, t_{mn} , between the m and the n Ti ions,

$$H_{mn}^{\text{tun}} = \sum_{ij} t_{mn}^{ij} d_{mi}^\dagger d_{nj} + \text{h.c.}, \quad (7)$$

where the indices i and j enumerate the eigen-orbitals of H_{mn}^{cf} (see Table III). The spin-orbit coupling is given by

$$H_{mn}^{\text{so}} = \lambda \sum_{k=m,n} \mathbf{l}_k \mathbf{s}_k, \quad (8)$$

where \mathbf{l}_k denotes the angular momentum operator of the Ti ion at the k site, \mathbf{s}_k its spin operator, and λ the spin-orbit coupling strength. We use $\lambda = 18 \text{ meV}$.¹⁴

The 14% reduction of the magnetic moment, alluded to in Sec. I above, is obtained upon diagonalizing together H_{mn}^{cf} and H_{mn}^{so} for a single Ti^{3+} ion. The reduction in the magnetic moment due to the not fully quenched orbital moment is estimated as follows. The spin along a certain selected direction does not commute with H_{mn}^{so} and therefore it is not a good quantum number for the combined Hamiltonian $H_{mn}^{\text{cf}} + H_{mn}^{\text{so}}$. However, the eigenstates of this combined Hamiltonian are symmetric or antisymmetric with respect to time-reversal. This leads to five Kramers doublets for the single Ti^{3+} ion. Since the ordered magnetic moment is mainly of the G-type, and is oriented along the x axis,⁴ we use those doublets to find the expectation values of the angular momentum. By choosing the largest possible polarization of the magnetic moment along the x axis out of all the linear combinations of the ground-state doublet, we find the expectation value $\langle l_k^x + 2s_k^x \rangle \mu_B = 0.86 \mu_B$. This effect is not included in our perturbation calculation of the magnetic exchange. However, it does explain partially why

the observed ordered moment along the x axis is reduced with respect to $1 \mu_B$.

The dominant hopping process between two nearest-neighbor Ti ions is mediated via the oxygen ion which is nearest to both of them. Let $t_m^{i\alpha}$ be the hopping matrix element of an electron in the p orbital α on the oxygen ion into the i state of the Ti ion located at m . The effective hopping between the Ti ions is then given by

$$t_{mn}^{ij} = -\frac{1}{\Delta_{\text{eff}}} \sum_{\alpha} t_m^{i\alpha} t_n^{j\alpha} = t_{nm}^{ji}. \quad (9)$$

Here, Δ_{eff} is the charge-transfer energy, which is required to put an electron from an O ion on a Ti ion, and α denotes one of the three p orbitals on the oxygen (in orthorhombic coordinates),

$$|x\rangle, |y\rangle, |z\rangle. \quad (10)$$

Using the structural data taken at $T = 8 \text{ K}$,⁴ together with elementary geometric considerations, the Ti–O hopping matrix elements can be expressed in terms of the Slater-Koster parameters $V_{pd\sigma}$ and $V_{pd\pi}$.²² We use the values $V_{pd\sigma} = -2.4 \text{ eV}$, $V_{pd\pi} = 1.3 \text{ eV}$, and $\Delta_{\text{eff}} = 5.5 \text{ eV}$,^{14,21} in conjunction with Eq. (9) to compute the effective hopping matrices pertaining to the unit cell. The results are listed in Table IV, which also gives the symmetry properties of the hopping matrices between different Ti–Ti bonds. The four inequivalent Ti sites of the unit cell form twelve nearest-neighbor Ti–Ti bonds which are crystallographically inequivalent, i.e. they do not evolve from each other by Bravais translations. These bonds connect the ten Ti ions indicated in Fig. 1. By the symmetry operations of the space group $Pbnm$, the eight effective hopping matrices between Ti ions belonging to the same ab plane and the four matrices for Ti–Ti bonds along the c direction, respectively, can be expressed by a single matrix each. For example, all twelve hopping matrices are given by the two matrices for the Ti–Ti bonds $mn = 12$ (planar) and $mn = 13$ (inter-planar), respectively.

Despite of the different orbital ordering within the ab planes and between them, the hopping amplitudes between the crystal-field ground states in and between the planes are of the same order of magnitude, i.e. roughly $|t_{12}^{00}| \approx |t_{13}^{00}|$. In strictly cubic symmetry, those are equal (see Appendix B). The rotation of the oxygen octahedra around the c axis, the tilting, and the distortion cause some difference between $|t_{12}^{00}|$ and $|t_{13}^{00}|$.

For convenience, we present in Table V an overview of the parameters used in our calculation.

C. The Ti–O hybridization

Our model does not include the covalent contribution to the crystal field, arising from hybridization between

the Ti-3*d* and O-2*p* states. This mechanism mixes excited states of the static crystal-field into the Ti³⁺ ground state, i.e., there is an admixture of Ti²⁺ states accompanied by an admixture of holes on the oxygen sites.

Following Ref. 21, we now estimate the effect of the *pd* hybridization. When that hybridization is absent, the effective parameter U_{eff} defines the energy difference between the ground state of the Ti³⁺ sector and the lowest state of the Ti²⁺ sector in a two-site cluster consisting of two Ti ions. When the *pd* hybridization is present, these two types of *d* states correspond to two bands, from which two *pd* hybridized bands evolve according to the covalent crystal field. These hybridized bands have, in general, considerable dispersion: Their peak-to-peak separation, which is seen in the combined photoemission and inverse photoemission spectra, is given by the band gap $E_{\text{gap}}=1.6\text{ eV}$, and the distance between the band edges is given by the optical gap $E_{\text{opt}}=0.2\text{ eV}$, which is experimentally observed as the Mott gap. The mean bandwidth between the two *pd* hybridized bands is then $W = E_{\text{gap}} - E_{\text{opt}} = 1.4\text{ eV}$.

Since the bands are rather dispersive, the question arises whether a localized picture is suitable to describe, even approximately, the LaTiO₃ system. In order to study this point, we have analyzed the covalent crystal field of a cluster consisting of a single Ti ion, and the six oxygen ions predominantly hybridized with it (the calculation has been carried out for Ti No. 1 in Fig. 1). This is accomplished by diagonalizing the Hamiltonian

$$H_{pd} = H^{\text{cf}} + H^{\text{c}} + H_{pd}^{\text{tun}}, \quad (11)$$

for a TiO₆-cluster. Here H^{cf} describes the static crystal field, H^{c} is the Coulomb interaction, and H_{pd}^{tun} is the *pd*-tunnelling,

$$H_{pd}^{\text{tun}} = \sum_{n\alpha} \tilde{t}_{1n}^{i\alpha} a_{1i}^{\dagger} p_{n\alpha} + \text{h. c.} \quad (12)$$

In Eq. (12), $p_{n\alpha}$ destroys an electron on the *n*-th oxygen site in the α -orbital, given in Eq. (10). As in the calculation of the Ti-Ti hopping amplitudes, the *pd* hopping amplitudes, $\tilde{t}_{1n}^{i\alpha}$, are expressed in terms of the Slater-Koster parameters $V_{pd\sigma}$ and $V_{pd\pi}$, using the structural data of Ref. 4. The entire space of the basis states of the TiO₆-cluster consists of a Ti³⁺ sector where the *p* orbitals are all occupied, and a Ti²⁺ sector where there is a hole in one of the *p* orbitals. The eigenstates of the Hamiltonian (11) have the form

$$|\psi\rangle = \sqrt{2-n_d} |d^1\rangle + \sqrt{n_d-1} |d^2\rangle, \quad (13)$$

where n_d is the occupation number of the Ti-*d* shell ($1 \leq n_d \leq 2$), $|d^1\rangle$ is a state with a single electron in the *d* shell and fully occupied *p* shells on the surrounding oxygen ions, and $|d^2\rangle$ is a state with two electrons in the *d* shell and a hole in the *p* shell of one of the oxygen ions. We find that in the ground state $n_d = 1.334$, i.e.,

there is a *p* hole on one of the neighboring oxygens with probability of 33.4%.

This calculation allows for the analysis of the eigenstates of the combined static and covalent crystal fields. Projecting the five lowest eigenstates onto the Ti³⁺ sector, (which corresponds to the states $|d^1\rangle$), gives to a very good approximation the same eigenstates as for the static crystal field alone, see Table VI. This finding explains why, despite the admixture of Ti²⁺ states $|d^2\rangle$, the agreement with the experiment remains perfect, as evidenced in Eq. (4). Indeed, the experiment measures the Ti³⁺ part, $|d^1\rangle$, of the combined static and covalent crystal field, and apparently is not sensitive to the Ti²⁺ admixture $|d^2\rangle$. Table VI also shows that the t_{2g} splitting remains almost the same as in the absence of the covalent contribution, whereas the distance between the t_{2g} and e_g energies is enhanced.

Since it is extremely complicated to include in the magnetic superexchange calculation the hopping between the *pd* hybridized states, we choose to consider the hopping between the Ti³⁺ states only. The results listed in Table VI, which show that the projections of the eigenstates of the combined static and covalent crystal fields onto the Ti³⁺ sector are almost the same as in the static-only case, ensure that the Ti³⁺ states we use are an appropriate starting point for the superexchange calculation.

D. Comparison with other models

It is instructive at this point to dwell on several differences between our model and three other calculations, reported in Refs. 7, 14, and 23.

(i) As is mentioned above, Ref. 14 takes into account the crystal field due to the La ions only. In addition, the intra-ionic Coulomb correlations are approximated according to the Kanamori scheme, which ignores the splitting of the spin-triplet states. As opposed to this calculation, we take into account the crystal field for both the Ti³⁺ and the Ti²⁺ configurations, and employ the full intra-ionic Coulomb correlations for the latter. The last point is particularly important: The spin-triplet states as intermediate Ti²⁺ states cause a ferromagnetic coupling while the spin-singlet states induce an antiferromagnetic coupling, leading to a competition between ferromagnetic and antiferromagnetic contributions to the magnetic exchange. On the other hand, we omit the small *pp* hybridization between the oxygen states, which was included in the calculation of Ref. 14.

(ii) The LDA+DMFT calculation⁷ gives a ground state (denoted here $|0''\rangle$) whose projection on the experimentally-deduced ground state, Eq. (3), is $|\langle 0'|0''\rangle|^2 = 87.8\%$, whereas we find 99.06%, see Eq. (4). An even larger difference, (which is partially explained by the difference in the ground-state orbitals) is found between the nearest-neighbor hopping amplitudes, coupling the Ti ions in that ground state: The values

cited in Ref. 7 are about half of the ones we use, with the in-plane amplitude being slightly smaller than the inter-plane one.

(iii) A recent calculation of the crystal field at room temperature, including the covalency contribution and the spin-orbit coupling,²³ has yielded basically the same t_{2g} splitting scheme as ours (due to Table VI), whereas the spacing between the t_{2g} and e_g states turned out to be bigger than in our calculation, about 0.9 eV. Analogously to the way we determined the reduction of the magnetic moment due to the spin-orbit coupling in Sec. II B, the ground state found in Ref. 23 has entangled spin-up and spin-down states, i.e. the orbital part is not separable from the spin part. The ground state is given there in the fashion which has the largest possible magnetic polarization along the quantization axis. Denoting the spin-up part of this ground state by $|0'''\rangle$, it turns out that the squared overlap with the experimentally determined orbital is $|\langle 0' | 0''' \rangle|^2 = 92.47\%$. In Ref. 23 the reduction of the G-type moment due to the crystal field and the spin-orbit coupling is found to be 9.5%, whereas we find 14%, see Sec. II B.

We will continue the comparison with other models when we discuss results of our calculation in Sec. IV.

III. THE EFFECTIVE SPIN HAMILTONIAN

Our aim is to obtain from the full Hamiltonian, $H_{mn} = H_{mn}^0 + V_{mn}$, an effective spin Hamiltonian, h_{mn} , which acts within the Hilbert space of the four-fold degenerate ground state of the unperturbed Hamiltonian H_{mn}^0 .

In general, an operator which acts in the ground-state space of the two Ti ions located at sites m and n , consists of linear combinations of following terms,

$$d_{m0\sigma'_m}^\dagger d_{n0\sigma'_n}^\dagger d_{n0\sigma_n} d_{m0\sigma_m}, \quad (14)$$

where $d_{n0\sigma_n}^\dagger$ ($d_{n0\sigma_n}$) creates (destroys) an electron in the crystal-field ground state at site n , of spin component σ_n . Since there is a single electron at each Ti site, the creation and annihilation operators can be written in terms of site spin-1/2 operators, \mathbf{S}_n ,

$$\begin{aligned} d_{n0\uparrow}^\dagger d_{n0\downarrow} &= S_n^+, \quad d_{n0\downarrow}^\dagger d_{n0\uparrow} = S_n^-, \\ d_{n0\uparrow}^\dagger d_{n0\uparrow} &= \frac{1}{2} + S_n^z, \quad d_{n0\downarrow}^\dagger d_{n0\downarrow} = \frac{1}{2} - S_n^z. \end{aligned} \quad (15)$$

Any operator acting within the ground-state space of the two Ti ions can be represented in terms of the 16 operators

$$\begin{aligned} &1 \text{ (constant),} \\ &S_k^\alpha \text{ (single-ion anisotropies),} \\ &S_m^\alpha S_n^\beta \text{ (inter-site spin couplings),} \end{aligned} \quad (16)$$

where $k = m, n$ and $\alpha, \beta = x, y, z$. Since the Hamiltonian is invariant under time-reversal, there are no single-ion

anisotropies, and consequently the effective spin Hamiltonian (omitting constant terms) takes the form

$$h_{mn} = \mathbf{S}_m A_{mn} \mathbf{S}_n, \quad (17)$$

where A_{mn} ($= A_{nm}^t$) is the 3×3 superexchange matrix. This matrix may be decomposed into a symmetric part and an antisymmetric one. The three components of the latter constitute the Moriya vector \mathbf{D}_{mn} ($= -\mathbf{D}_{nm}$). Extracting further the isotropic part of A_{mn} , i.e., the Heisenberg coupling J_{mn} , the effective spin Hamiltonian is cast into the form

$$h_{mn} = J_{mn} \mathbf{S}_m \mathbf{S}_n + \mathbf{D}_{mn} (\mathbf{S}_m \times \mathbf{S}_n) + \mathbf{S}_m A_{mn}^s \mathbf{S}_n. \quad (18)$$

Here, A_{mn}^s represents the symmetric anisotropy. Due to the space-group symmetries, all three types of magnetic couplings belonging to the eight planar Ti-Ti bonds may be obtained from those of a single bond, and so is the case for the four inter-planar bonds, see Table VII.

The various magnetic couplings appearing in Eq. (18) are obtained by perturbation theory to leading order in V_{mn} , namely, to second order in the hopping t_{mn} and to first and second order in the spin-orbit coupling (scaled by λ). In order to accomplish this calculation, we introduce the projection operator P_{mn}^0 onto the ground-state of H_{mn}^0 , and the combined resolvent and projection operator S_{mn} onto the excited states.²⁴ In terms of these projection operators, the various terms appearing in Eq. (18) acquire the following structure. The Heisenberg isotropic exchange, to leading order in the Ti-Ti hopping, is

$$J_{mn} \mathbf{S}_m \mathbf{S}_n = P_{mn}^0 H_{mn}^{\text{tun}} S_{mn} H_{mn}^{\text{tun}} P_{mn}^0. \quad (19)$$

The second term in Eq. (18) is the Dzyaloshinskii-Moriya antisymmetric anisotropic exchange interaction, which arises from second-order processes in the tunnelling Hamiltonian, and first-order processes in the spin-orbit coupling,

$$\begin{aligned} \mathbf{D}_{mn} (\mathbf{S}_m \times \mathbf{S}_n) &= P_{mn}^0 H_{mn}^{\text{tun}} S_{mn} H_{mn}^{\text{tun}} S_{mn} H_{mn}^{\text{so}} P_{mn}^0 \\ &+ P_{mn}^0 H_{mn}^{\text{so}} S_{mn} H_{mn}^{\text{tun}} S_{mn} H_{mn}^{\text{tun}} P_{mn}^0. \end{aligned} \quad (20)$$

In fact, there are additional terms in this order, in which there appear two Ti^{2+} resolvents, e.g., $P_{mn}^0 H_{mn}^{\text{tun}} S_{mn} H_{mn}^{\text{so}} S_{mn} H_{mn}^{\text{tun}} P_{mn}^0$. These are smaller than the ones we keep, by an additional factor of $\simeq \Delta_{\text{cf}}/U_{\text{eff}} = 0.059$, where $\Delta_{\text{cf}} = 0.208$ eV is the gap between the ground state of the single-particle crystal field and the first excited state, see Table III. Following Ref. 25, we denote the vectors \mathbf{D}_{mn} , which refer to the microscopic single-bond couplings of the spins, as the Moriya vectors. The macroscopic antisymmetric anisotropic couplings between the sublattice magnetizations of the classical ground state (discussed in the next section) are referred to as the Dzyaloshinskii vectors. They are related to the Moriya vectors but are not necessarily the same.

Finally, processes which are second-order in both the tunnelling and the spin-orbit interaction, yield

$$\begin{aligned}
\mathbf{S}_m A_{mn}^s \mathbf{S}_n + \mathbf{D}'_{mn} (\mathbf{S}_m \times \mathbf{S}_n) = & P_{mn}^0 H_{mn}^{\text{so}} S_{mn} H_{mn}^{\text{tun}} S_{mn} H_{mn}^{\text{tun}} S_{mn} H_{mn}^{\text{so}} P_{mn}^0 \\
& + P_{mn}^0 H_{mn}^{\text{so}} S_{mn} H_{mn}^{\text{so}} S_{mn} H_{mn}^{\text{tun}} S_{mn} H_{mn}^{\text{tun}} P_{mn}^0 + P_{mn}^0 H_{mn}^{\text{tun}} S_{mn} H_{mn}^{\text{tun}} S_{mn} H_{mn}^{\text{so}} S_{mn} H_{mn}^{\text{so}} P_{mn}^0 \\
& + P_{mn}^0 H_{mn}^{\text{so}} S_{mn}^2 H_{mn}^{\text{so}} P_{mn}^0 H_{mn}^{\text{tun}} S_{mn} H_{mn}^{\text{tun}} P_{mn}^0 + P_{mn}^0 H_{mn}^{\text{tun}} S_{mn} H_{mn}^{\text{tun}} P_{mn}^0 H_{mn}^{\text{so}} S_{mn}^2 H_{mn}^{\text{so}} P_{mn}^0.
\end{aligned} \tag{21}$$

These terms give rise to the symmetric anisotropies A_{mn}^s , as well as to corrections \mathbf{D}'_{mn} , of order λ^2 , to the Moriya vectors. We have again omitted terms including two Ti^{2+} resolvents.

As was shown in Ref. 25, a systematic description of the magnetic anisotropies due to the spin-orbit interaction requires both the first and the second order processes in λ . The technical reason being that the expectation value of the cross product in the second term of Eq. (18) is, in fact, also of order λ , so that altogether the Dzyaloshinskii-Moriya interaction is at least second order in the spin-orbit coupling. As a result, although the antisymmetric Dzyaloshinskii-Moriya interaction alone gives rise to spin-canting, when taken together with the symmetric anisotropy, the system may, under specific conditions, still preserve rotational invariance of the spins.

The detailed calculation of the various terms appearing in Eqs. (19), (20), and (21) is lengthy, albeit straightforward. More details are given in Appendix C. The values we obtain, using the parameters cited above, are listed in Table VIII. A comparison with spin-wave measurements is given at the end of the following section.

IV. THE CLASSICAL GROUND STATE

A. The magnetic order of the classical ground state

The single-bond spin Hamiltonian, Eq. (18), is the basis for the magnetic Hamiltonian, from which the magnetic order of the classical ground state follows. To construct the latter, the entire Ti-lattice is decomposed into four sublattices. Namely, each magnetic unit cell includes four Ti ions, just as the crystallographic unit cell. The four sublattices are hence enumerated according to the numbers of the four Ti ions per unit cell shown in Fig. 1 (sublattice $i = 1$ corresponds to Ti ion 1 and its Bravais translations, etc.). Assigning a fixed-magnitude magnetization (per site) to each sublattice, \mathbf{M}_i , one sums over all bonds which couple the four sublattices, to obtain the *macroscopic* magnetic Hamiltonian in the form

$$H_M = \sum_{ij} [I_{ij} \mathbf{M}_i \mathbf{M}_j + \mathbf{D}_{ij}^D (\mathbf{M}_i \times \mathbf{M}_j) + \mathbf{M}_i \Gamma_{ij} \mathbf{M}_j], \tag{22}$$

where ij runs over the sublattice pairs 12, 13, 24, and 34 of Fig. 1. This summation procedure gives rise to the macroscopic magnetic couplings: I_{ij} is the macroscopic isotropic coupling, \mathbf{D}_{ij}^D are the Dzyaloshinskii vectors (to

leading order in the spin-orbit coupling λ), which are the macroscopic antisymmetric anisotropies, and Γ_{ij} are the macroscopic symmetric anisotropy tensors (of order λ^2). The relations between those macroscopic couplings and the microscopic single-bond couplings are listed in Table IX. The inter-relations among the macroscopic couplings, which are dictated by the symmetries of the space-group, are contained in Table X.

Although all four sublattice magnetizations are of equal magnitudes, their directions are all different. Those determine the magnetic structure of the classical ground state. In general, according to the space group $Pbnm$ symmetries, there are four possibilities for the symmetry of sublattice magnetizations of the classical ground state, as listed in Table XI.² In our case, the minimization of the magnetic Hamiltonian, Eq. (22), yields the magnetic structure shown in Fig. 3, drawn according to Table XII. This ground state has the following symmetry: The x components of the magnetizations order antiferromagnetically, in a G-type structure. The y components order antiferromagnetically as well, but in an A-type structure. Finally, the z components of the magnetizations order ferromagnetically. Consequently, the classical ground state is characterized by two canting angles, φ and ϑ , whose values are given in Table XIII, (see also Fig. 3). Due to the dominating Heisenberg coupling one observes that the magnetic structure of the classical ground state is predominantly G-type. The easy direction along the x axis and the canting angles (both proportional to the spin-orbit coupling λ) result from the anisotropic couplings of the model. Those break the rotational invariance of the magnetizations, and also cause the deviations from the pure G-type structure.

Our magnetic structure is fully consistent with the experimental one, as reported in Ref. 4. This experiment (in contrast to the one reported in Ref. 2) reveals that the G-type structure is indeed along the x direction, while the ferromagnetic moment is along the z direction. Moreover, since the experiment of Ref. 4 is not sensitive to a small moment along the y axis,²⁶ our small A-type antiferromagnetic order along this direction does not contradict the data. We emphasize again that symmetry allows for such ordering, given the G-type order along x and the ferromagnetic order along z . Indeed, in the YTiO_3 -system, which has the same space group as LaTiO_3 , such order has been detected,²⁷ but with different magnitudes of the canting angles, which cause the ferromagnetic order to dominate.

One should note that by using naively the procedure outlined above to obtain the energy of the classical

magnetic ground-state, one obtains in the energy non-systematic contributions up to fourth order in the spin-orbit coupling λ . To exemplify this point, we consider

$$\begin{aligned}
\langle H_M \rangle = & [\lambda^0:] -2(I_{12} + I_{13}) \cos^2 \varphi \cos^2 \vartheta \\
& [\lambda^2:] +2(I_{12} - I_{13}) \sin^2 \varphi \cos^2 \vartheta + 2(I_{12} + I_{13}) \sin^2 \vartheta + 4(D_{12}^{Dy} + D_{13}^{Dy}) \cos \varphi \cos \vartheta \sin \vartheta \\
& + 4D_{12}^{Dz} \cos \varphi \sin \varphi \cos^2 \vartheta - 2(\Gamma_{12}^{xx} + \Gamma_{13}^{xx}) \cos^2 \varphi \cos^2 \vartheta \\
& [\lambda^3:] -4D_{13}^{Dx} \sin \varphi \cos \vartheta \sin \vartheta - 4\Gamma_{13}^{xy} \cos \varphi \sin \varphi \cos^2 \vartheta \\
& [\lambda^4:] +2(\Gamma_{12}^{yy} - \Gamma_{13}^{yy}) \sin^2 \varphi \cos^2 \vartheta + 2(\Gamma_{12}^{zz} + \Gamma_{13}^{zz}) \sin^2 \vartheta - 2\Gamma_{12}^{yz} \sin \varphi \cos \vartheta \sin \vartheta.
\end{aligned} \tag{23}$$

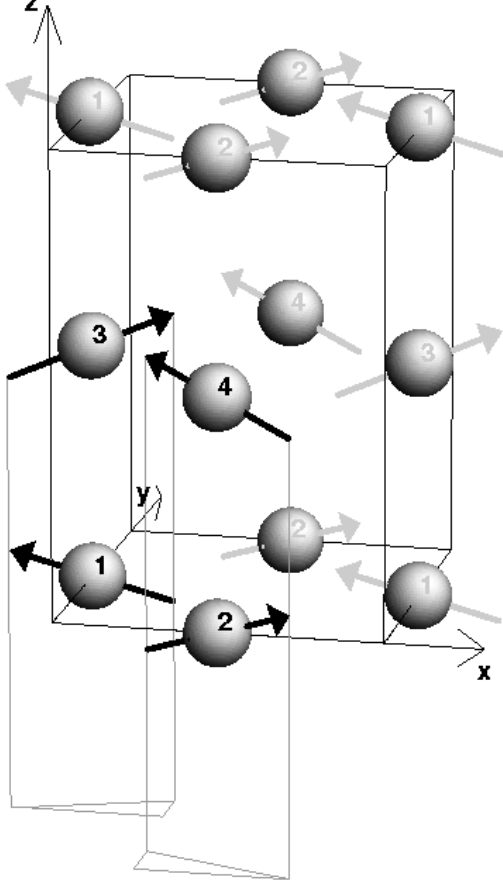


FIG. 3. The magnetic order of the Ti ions in the classical ground state of the effective spin Hamiltonian of the lattice. The ions are enumerated according to the sublattice to which they belong. The x components of the spins order antiferromagnetically in the G-type configuration, the y components order antiferromagnetically in the A-type one, and the z components order ferromagnetically.

The leading orders of the terms are indicated in the square brackets. The non-systematic contributions of fourth order in λ are due to the couplings Γ_{12}^{yy} , Γ_{13}^{yy} , Γ_{12}^{zz} , Γ_{13}^{zz} , Γ_{12}^{yz} (which are all of order λ^2 but are multiplied by $\sin^2 \vartheta$, $\sin^2 \varphi$ and $\sin \vartheta \sin \varphi$ which are also of order λ^2), and the λ^2 correction of D_{13}^{Dx} (which is multiplied by $\sin \vartheta \sin \varphi$). Those contributions have been *excluded* from

the expectation value of H_M for the Ti-ions pairs $ij = 12$ and 13, expressed in terms of the angles φ and ϑ and the superexchange couplings,

our calculation of the canting angles. On the other hand, we do include in the minimization of $\langle H_M \rangle$ terms up to the third order in λ . This implies a systematic derivation of the canting angles to first order in this coupling. (The classical ground-state energy has been found consistently, term by term, to second order in λ . Although Γ_{12}^{xx} and Γ_{13}^{xx} have been calculated only up to order λ^2 and consequently, we do not have the complete third-order term, this is of little importance when the canting angles are determined, since those couplings appear only with $\cos \vartheta$ and $\cos \varphi$, and therefore just cause an energy shift in $\langle H_M \rangle$.) Note also that although the Dzyaloshinskii and Moriya vectors first appear in linear order in λ and the symmetric anisotropy coefficients in quadratic order, *both kinds of anisotropies* have to be considered as they cause terms which contribute in the same order of λ to the classical ground-state energy.

The values we obtain for the angles φ and ϑ are listed in Table XIII. In particular, $\vartheta = 0.80^\circ$, agrees, within the experimental error, with the values reported in Refs. 2 and 11, 0.85° and 1.5° , respectively. (Note that ϑ is defined here with respect to the ab plane.) This canting angle causes the weak ferromagnetic moment, of order $0.014 \mu_B$. This value agrees with the experimental one, within the uncertainty of the measurements which is caused by twinning of the crystal.²⁸

Recently, an attempt has been made to analyze the relation between the anisotropy of the spin couplings and the paramagnetic susceptibility, which also has some anisotropy.²³ In this work the anisotropy of the spin couplings is taken into account by postulating phenomenologically an xyz model, which couples neighboring Ti spins and corresponds in our calculation to the coefficients \mathbf{A}_{mn}^d from Table VIII. A model susceptibility, which results from the xyz coupling via a molecular-field approximation (and from single-ion as well as from covalence effects), is calculated and then fitted with a couple of free parameters onto the measured susceptibility. As we have shown in this section, the antisymmetric and off-diagonal symmetric anisotropies—in the particular case of Eq. (23), components of the Dzyaloshinskii vectors and Γ_{13}^{xy} —can have at least the same conceptual importance for the magnetic properties of LaTiO_3 as the xyz anisotropies. Alternatively spoken, in general the xyz anisotropy is not the dominant anisotropy. This

basic argument is not restricted to the low-temperature case, which is accompanied by the magnetic order and which we investigate in the present paper, but refers also to the underlying spin couplings which influence high-temperature properties like the paramagnetic susceptibility (whereas, e. g., the difference between the structural parameters of the low- and high-temperature case might correspond to more or less slight differences of the spin-coupling coefficients and of the orbital ground state). In the way of an extension of Ref. 23, the question whether it is possible to include also the other than *xyz* anisotropies via free parameters in a model susceptibility and to compare this susceptibility to experiment, might be interesting.

B. Comparison with spin-wave data

The magnetic order in the classical ground state is the common starting point for a spin-wave calculation. In the case of the spin Hamiltonian pertaining to LaTiO_3 , Eq. (18), one expects a rich spin-wave spectrum. This calculation is currently being undertaken, and will be presented elsewhere.²⁹ Nevertheless, our results above may be roughly compared with the existing spin-wave data. To this end, we ignore the antisymmetric and the symmetric anisotropies and hence assume a classical Néel state (for which the spin-wave spectrum is gapless).

Inelastic neutron scattering has yielded the same value, $J = 15.5 \text{ meV}$, for the *single-bond* Heisenberg coupling for both the Ti–Ti bonds in the *ab* planes and those in-between the planes.⁶ This value has been confirmed by the evaluation of Raman spectra.³⁰ Were we to average our calculated values over the six bonds of each Ti ion, we would have obtained a value which is 32 % higher. This rather modest discrepancy can be easily removed, by fine-tuning the model parameters. For example, by using the value $\Delta_{\text{eff}} = 6.6 \text{ eV}$ (as estimated from an LDA+DMFT calculation based on the recent structural data³¹), or by using a smaller value for the Slater-Koster parameters, $V_{pd\sigma} = -2.2 \text{ eV}$ (keeping the ratio between those parameters fixed, $V_{pd\pi} = 1.2 \text{ eV}$) instead of -2.4 eV ,⁵ or any other combined reduction of both of these parameters. Since a detailed comparison with the data requires the full spin-wave calculation, we do not attempt here any fine-tuning of the model parameters. For the purpose of the present paper, it suffices that the calculated Heisenberg couplings are consistent with the experimental value, within the uncertainties of our model parameters.

Our calculation predicts somewhat different values for the in-plane Heisenberg coupling, J_{12} , and the out-of-plane one, J_{13} , yielding the ratio $\delta = J_{13}/J_{12} \simeq 79 \%$. Such an anisotropy may be detected by comparing with the spin-wave dispersion, $\epsilon(\mathbf{q})$, at selected points, $\mathbf{q} = (0, 0, \pi)$ and $\mathbf{q} = (\pi, 0, 0)$, in the Brillouin zone of an effective cubic lattice of a unit lattice constant. When

only this anisotropy is taken into account, then linear spin-wave theory gives

$$\epsilon(\mathbf{q}) = J_{12} \sqrt{(2 + \delta)^2 - (\cos q_x + \cos q_y + \delta \cos q_z)^2}. \quad (24)$$

With our calculated δ , we find $\epsilon(0, 0, \pi)/\epsilon(\pi, 0, 0) = 94 \%$, well within the experimental error bar of about 10 % for the spin-wave energies, from which the equality of the Heisenberg couplings on all bonds has been deduced.³² Hence, the (approximate) isotropy of the spin-wave spectrum due to Ref. 6, which has been used as an argument to support the orbital-liquid state,³ is consistent with our model.

The calculation of Ref. 14 yielded a different value for the Heisenberg coupling ratio, $\delta = 106 \%$, i. e. a larger coupling along the *c* axis. This discrepancy can be traced back to our different crystal-field spectrum. In our case, the hopping amplitude between the crystal-field ground states on neighboring Ti ions is about 10 % smaller for the bond 13 than for 12, see Table IV. This is a geometric effect which follows from the structural data.⁴

From a fit to the observed spin-wave gap, of order $\Delta = 3.3 \text{ meV}$, in conjunction with a spin model including *solely* antisymmetric anisotropies, a value of $D = 1.1 \text{ meV}$ has been deduced for the magnitude of the Moriya vectors.⁶ We obtain higher magnitudes for the Moriya vectors. However, a full spin-wave expansion based on the Hamiltonian (18) indicates that the spin-wave gap is in fact dominated by the symmetric anisotropies rather than by the antisymmetric ones.²⁹ It is the canting of the ordered spins with respect to each other which is dominated by the Dzyaloshinskii vectors.

V. SUMMARY

We have presented a detailed analysis of the magnetic order pertaining to the LaTiO_3 system. The starting point of our calculation is the Ti-*d* orbital configuration which results from the static crystal field that includes the Jahn-Teller distortion, and which gives rise to orbital ordering as found in the experiment.⁴ This orbital ordering rules out the orbital-liquid picture³ for LaTiO_3 , which ignores the Jahn-Teller-like t_{2g} splitting scheme and the resulting non-degenerate orbital ground state.

Employing a perturbation expansion of this non-degenerate ground state in the effective hopping between neighboring Ti-ions, and in the on-site spin-orbit coupling, we have derived an effective spin Hamiltonian. It includes, in addition to the Heisenberg isotropic interaction between nearest-neighbor Ti-ions, the antisymmetric Dzyaloshinskii-Moriya coupling, and the symmetric anisotropic coupling. These three interactions conspire together to yield the magnetic order. We have found, by minimizing the magnetic energy of the classical ground state, that the magnetic order is primarily that of a G-type antiferromagnet, with the ordered moment along the

crystallographic a axis, accompanied by a weak ferromagnetic moment along the c axis. This configuration is in good agreement with the experimental findings. In addition, we have found that there is a small A-type moment of the spin components along the b axis, which (although not yet detected in experiment) is allowed by the symmetry of the system. We find that the in-plane Heisenberg coupling energy is about 27% higher than that pertaining to the coupling between ab -planes. By using these values in a spin-wave theory for the Heisenberg couplings, we show that both couplings are consistent with the isotropic spin-wave dispersion measured by inelastic neutron scattering.⁶

Our method seems to be particularly suitable to describe the ferromagnetic Mott insulator YTiO_3 as well.

APPENDIX A: THE EWALD SUMMATION

The Madelung sum for the Coulomb potential in the point-charge model is given by

$$V(\mathbf{r}) = -e \sum_{\mathbf{l}, n}^{\prime} \frac{q_n}{|\mathbf{l} + \mathbf{a}_n - \mathbf{r}|}, \quad (\text{A1})$$

where $\mathbf{r} = (x, y, z)$ is a point on the Ti ion No. 1, whose center is taken as the origin. In Eq. (A1), \mathbf{l} are the

$$V(\mathbf{r}) = -e \sum_{\mathbf{g} \neq 0} \frac{4\pi}{V_e g^2} e^{-\frac{g^2}{4G^2} + i\mathbf{g}\mathbf{r}} \sum_n q_n e^{-i\mathbf{g}\mathbf{a}_n} - e \sum_{\mathbf{l}, n}^{\prime} \frac{q_n}{|\mathbf{l} + \mathbf{a}_n - \mathbf{r}|} \text{erfc}(G|\mathbf{l} + \mathbf{a}_n - \mathbf{r}|) + e \frac{q_1}{r} \text{erf}(Gr). \quad (\text{A2})$$

Here \mathbf{g} are the vectors of the reciprocal Bravais lattice, whose basis vectors are $(2\pi/a, 0, 0)$, $(0, 2\pi/b, 0)$, and $(0, 0, 2\pi/c)$, $V_e = abc$ is the volume of the unit cell, and G is a frequency cutoff. The value of $V(\mathbf{r})$ is of course independent of G . This cutoff is chosen such that the sum over the real-space lattice and the one over the reciprocal lattice can be stopped after about the same number of sites, when the required numerical precision is reached. In Eq. (A2), erf and erfc are the error functions

$$\text{erf}(z) = 1 - \text{erfc}(z) = \frac{2}{\sqrt{\pi}} \int_0^z e^{-t^2} dt. \quad (\text{A3})$$

The Ewald construction requires the neutrality condition

$$\sum_n q_n = 0, \quad (\text{A4})$$

which is fulfilled in our case.

In order to find the spectrum and the eigenstates of the static crystal field, we have replaced the potential $V(\mathbf{r})$ by the pseudo-potential $V_{\text{ps}}(\mathbf{r})$, which is its Taylor expansion including the second and fourth orders in \mathbf{r} . These are the Taylor orders which have non-trivial matrix elements with respect to the d orbitals.³⁵ For instance, the second (fourth) Taylor order includes also terms which

Preliminary calculations (to be presented elsewhere) indeed indicate ferromagnetic couplings in the ab -planes.²⁹ Since the covalent pd hybridization in this system is as strong as in LaTiO_3 , it will be of much interest to compare the classical magnetic Hamiltonians of the two systems, and the ensuing spin-wave spectra.

VI. ACKNOWLEDGMENTS

We gratefully acknowledge discussions with M. Braden, L. Craco, M. Cwik, M. Grüninger, B. Keimer, D.I. Khomskii, and L.H. Tjeng. This work was supported by the German-Israeli Foundation for Research (GIF).

Bravais translations, \mathbf{a}_n are the basis vectors of the unit cell, and q_n are the corresponding point charges. The prime on the sum symbol indicates that the ion at the origin, $\mathbf{l} = \mathbf{a}_n = \mathbf{0}$, is omitted. This sum converges very slowly. One therefore uses the Ewald summation,³³ (see also Ref. 34) where the sum (A1) is mapped onto two sums which converge much better, and which can be computed to high accuracy. Using the Ewald summation, the Madelung potential can be expressed in the form

are proportional to xy (x^3y, x^2y^2). For the Taylor expansion we use ($r = |\mathbf{r}|$)

$$\frac{1}{r} \text{erf}(Gr) = \frac{2G}{\sqrt{\pi}} \left[1 - \frac{(Gr)^2}{3} + \frac{(Gr)^4}{10} + \dots \right]. \quad (\text{A5})$$

The potential $V_{\text{ps}}(\mathbf{r})$ is a harmonic function, invariant under inversion of the coordinates. The diagonalization of the matrix $\langle \gamma | V_{\text{ps}}(\mathbf{r}) | \gamma' \rangle$, where γ and γ' denote the orthorhombic d orbitals, gives the results listed in Table III for the static crystal field. This calculation requires the second and fourth moments of the effective ionic radius, defined by

$$\int f^2(r) r^{2+n} dr = \langle r^n \rangle, \quad n = 2, 4, \quad (\text{A6})$$

where $f(r)$ denotes the radial part of the d -orbitals.¹⁶

APPENDIX B: THE HOPPING AMPLITUDES BETWEEN THE CRYSTAL-FIELD GROUND STATES

As is mentioned in the text, the effective Ti-Ti hopping matrix elements between the crystal-field ground states

in the ab planes are of the same order of magnitude as those between planes, i.e., $|t_{12}^{00}| \approx |t_{13}^{00}|$. This is a somewhat surprising result in view of the fact that there is ferro-orbital order in the planes and (canted) antiferro-orbital order between them. However, as we show here, in strictly cubic symmetry one has $|t_{12}^{00}| = |t_{13}^{00}|$. The deviations from cubic symmetry cause the slight difference between these two hopping amplitudes.

Let us hence consider the cubic case, and employ the coordinate system x', y', z in which the Ti sites 1 and 2 are on the x' axis (see Fig. 1; these coordinates are rotated by 45° compared to the orthorhombic ones). The crystal-field ground states are now linear combinations of the three degenerate t_{2g} orbitals

$$|y'z\rangle, |x'z\rangle, |x'y'\rangle. \quad (\text{B1})$$

The hopping amplitudes are proportional to the overlap of the two pertaining orbitals. Let us consider for simplicity the base-orbitals according to Eq. (3), i.e.,

$$\begin{aligned} |1\rangle &= |2\rangle = \frac{1}{\sqrt{3}}(|y'z\rangle - |x'z\rangle + |x'y'\rangle), \\ |3\rangle &= \frac{1}{\sqrt{3}}(-|y'z\rangle + |x'z\rangle + |x'y'\rangle), \end{aligned} \quad (\text{B2})$$

where 1, 2 and 3 denote the relevant Ti-ions (see Fig. 1). Were we to find the direct hopping between the Ti sites, we would have obtained for the overlaps the result

$$\langle 1|2\rangle = 1, \quad \langle 1|3\rangle = -\frac{1}{3}, \quad (\text{B3})$$

which reflects the ferro-orbital and nearly antiferro-orbital order, respectively. However, the *effective* Ti-Ti hopping that we consider is mediated by the oxygens located between the Ti ions. Then, in strictly cubic symmetry, for each pair of Ti ions, one of the three t_{2g} orbitals cannot hybridize. This ‘inactiveness’ of one of the orbitals³ is a direct consequence of the cubic symmetry, as is portrayed in Fig. 4, and is the source of peculiar hidden symmetries in the cubic Hamiltonian.^{12,13} In our example, the orbital $|y'z\rangle$ is inactive for the 12-bond, while for the bond 13 the inactive orbital is $|x'y'\rangle$, and consequently

$$\begin{aligned} \langle 1|2\rangle &\rightarrow \frac{1}{3}(-\langle x'z| + \langle x'y'|)(-|x'z\rangle + |x'y'\rangle) = \frac{2}{3}, \\ \langle 1|3\rangle &\rightarrow \frac{1}{3}(\langle y'z| - \langle x'z|)(-|y'z\rangle + |x'z\rangle) = -\frac{2}{3}, \end{aligned} \quad (\text{B4})$$

leading to $|t_{12}^{00}| = |t_{13}^{00}|$.

APPENDIX C: THE EXPLICIT CALCULATION OF THE EXCHANGE COUPLINGS

Here we document the technical details of the perturbation calculation, that yields the effective spin Hamiltonian.

As explained in Sec. II, we consider a cluster of two nearest-neighbor Ti ions. The Hamiltonian of this cluster, given in Eqs. (5) and (6), is expressed in terms of the

operators $d_{ki\sigma}^\dagger$ ($d_{ki\sigma}$) which create (destroy) an electron in the crystal-field eigen-orbital i with spin component σ , on the Ti ion located at site k . However, it is more convenient to treat the two-electron states (which appear in the intermediate stages of the perturbation expansion) using the orthorhombic basis, Eq. (1). We denote the operators pertaining to this basis by $c_{k\gamma\sigma}^\dagger$ ($c_{k\gamma\sigma}$), where γ enumerates the orthorhombic orbitals. The first part of this Appendix is devoted to the transformation of the Hamiltonian between the two schemes, and the diagonalization of the two-electron states. In the second part, we summarize the detailed expressions of the various terms resulting from the perturbation expansion.

1. The Hamiltonian

Denoting the matrix of the crystal-field Hamiltonian in the orthorhombic basis by $V(k)$, we have

$$H^{\text{cf}} = \sum_{k\gamma_1\gamma_2\sigma} V_{\gamma_1\gamma_2}(k) c_{k\gamma_1\sigma}^\dagger c_{k\gamma_2\sigma}. \quad (\text{C1})$$

The matrices $V(k)$ are real and symmetric. We next introduce the (unitary and real) matrix $W(k)$ which diagonalizes the crystal-field Hamiltonian, bringing it to the form

$$H^{\text{cf}} = \sum_{ki\sigma} E_i d_{ki\sigma}^\dagger d_{ki\sigma}, \quad (\text{C2})$$

where E_i are the crystal-field eigenvalues, listed in Table III. These single-particle energies are shifted so that $E_0 = 0$ eV, $E_1 = 0.209$ eV, etc. The relations between the operators $d_{ki\sigma}^\dagger$ and $c_{k\gamma\sigma}^\dagger$ are hence given by

$$d_{ki\sigma}^\dagger = \sum_{\gamma} W_{i\gamma}(k) c_{k\gamma\sigma}^\dagger, \quad c_{k\gamma\sigma}^\dagger = \sum_i W_{\gamma i}^t(k) d_{ki\sigma}^\dagger, \quad (\text{C3})$$

such that

$$W(k)V(k)W^t(k) = E, \quad (\text{C4})$$

with $E = \text{diag } E_i$. The diagonalizing matrix pertaining to site 1, $W(1)$, is given in Table III. All other $W(k)$ and $V(k)$ follow from the symmetry properties of the unit cell, and are given by

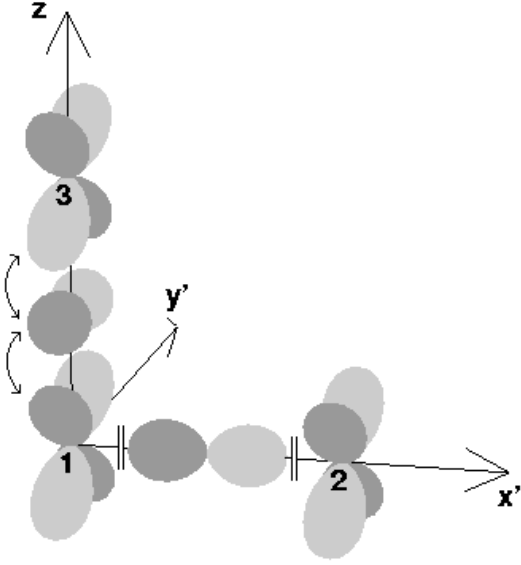
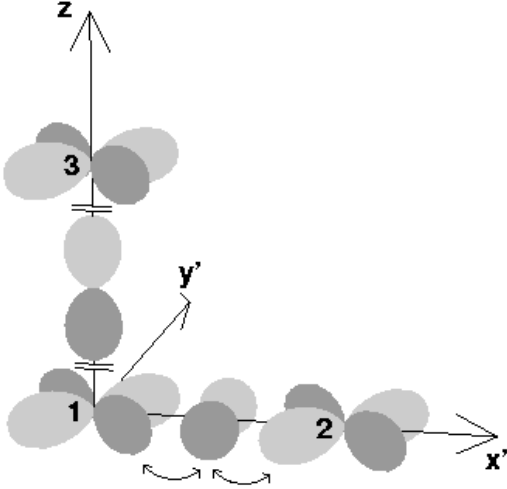
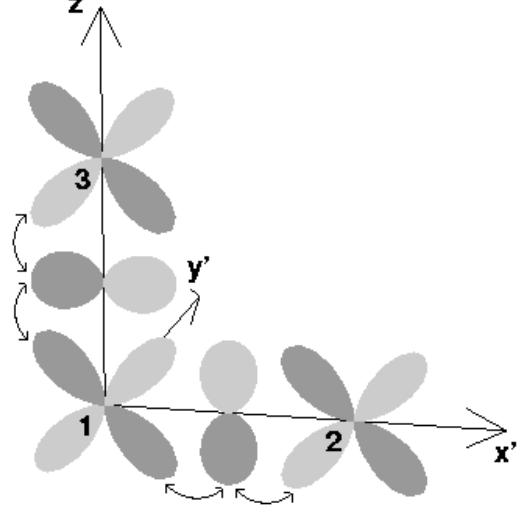
(a) The hopping between the orbitals $|y'z\rangle$ (b) The hopping between the orbitals $|x'y'\rangle$ (c) The hopping between the orbitals $|x'z\rangle$ 

FIG. 4. In cubic symmetry, there is one t_{2g} orbital per each Ti-O-Ti bond, which cannot participate in the hopping between the Ti and the O ions because of the parity of the O-2p orbitals. This is shown in panels (a)–(c), for each of the three t_{2g} orbitals, respectively. (a) The hopping between the orbitals $|y'z\rangle$ at the Ti sites 1 and 2 is not possible, since on the intermediate oxygen site there is no p orbital with a parity that would allow such hopping. For the same reason, an electron cannot hop from the p orbital $|x'\rangle$, which is shown between the Ti sites 1 and 2, to any of the t_{2g} orbitals of the Ti sites. On the other hand, the hopping between the orbitals $|y'z\rangle$ at the Ti sites 1 and 3, which is mediated by the orbital $|y'\rangle$ on the intermediate oxygen site, is possible. (b) Analogously to the case (a), the hopping between the orbitals $|x'y'\rangle$ at the Ti sites 1 and 3 is not permitted, because on the intermediate oxygen site there is no appropriate p orbital. Likewise, an electron cannot hop from the p orbital $|z\rangle$, which is shown between the Ti sites 1 and 3, to any of the t_{2g} orbitals of the Ti sites. The (allowed) hopping between the orbitals $|x'y'\rangle$ at the Ti sites 1 and 2 is mediated by the orbital $|y'\rangle$ on the intermediate oxygen site. (c) The hopping between the orbitals $|x'z\rangle$ at the Ti sites 1 and 2 is mediated by the orbital $|z\rangle$ on the intermediate oxygen site. The hopping between the orbitals $|x'z\rangle$ at the Ti sites 1 and 3 is mediated by the orbital $|x'\rangle$ on the intermediate oxygen site.

$$\begin{aligned}
W(2) &= \begin{bmatrix} - & + & + & - & + \\ - & + & + & - & + \\ - & + & + & - & + \\ - & + & + & - & + \\ - & + & + & - & + \end{bmatrix} \otimes W(1), \\
V(2) &= \begin{bmatrix} + & - & - & + & - \\ - & + & + & - & + \\ - & + & + & - & + \\ + & - & - & + & - \\ - & + & + & - & + \end{bmatrix} \otimes V(1), \\
W(3) &= \begin{bmatrix} + & + & - & - & + \\ + & + & - & - & + \\ + & + & - & - & + \\ + & + & - & - & + \\ + & + & - & - & + \end{bmatrix} \otimes W(1), \\
V(3) &= \begin{bmatrix} + & + & - & - & + \\ + & + & - & - & + \\ - & - & + & + & - \\ - & - & + & + & - \\ + & + & - & - & + \end{bmatrix} \otimes V(1), \quad (C5)
\end{aligned}$$

where we have used the direct matrix product $a = b \otimes c$, i.e., $a_{ij} = b_{ij}c_{ij}$.

$$\begin{aligned}
|1\rangle &= \Psi_T^{52}, |2\rangle = \Psi_T^{53}, |3\rangle = \Psi_T^{41}, |4\rangle = \Psi_T^{23}, |5\rangle = \Psi_T^{54}, \\
|6\rangle &= \Psi_T^{13}, |7\rangle = \Psi_T^{24}, |8\rangle = \Psi_T^{21}, |9\rangle = \Psi_T^{34}, |10\rangle = \Psi_T^{51}, \quad (C8)
\end{aligned}$$

the Coulomb Hamiltonian in the triplet sector becomes

$$U_T = \begin{bmatrix} A-8B & 0 & 0 & 0 & 0 & 0 & 0 & 0 & 0 & 0 \\ 0 & A-5B & 3B & 3B\sqrt{3} & 0 & 0 & 0 & 0 & 0 & 0 \\ 0 & 3B & A-5B & 3B\sqrt{3} & 0 & 0 & 0 & 0 & 0 & 0 \\ 0 & 3B\sqrt{3} & 3B\sqrt{3} & A+B & 0 & 0 & 0 & 0 & 0 & 0 \\ 0 & 0 & 0 & 0 & A-5B & 3B & -3B\sqrt{3} & 0 & 0 & 0 \\ 0 & 0 & 0 & 0 & 3B & A-5B & -3B\sqrt{3} & 0 & 0 & 0 \\ 0 & 0 & 0 & 0 & -3B\sqrt{3} & -3B\sqrt{3} & A+B & 0 & 0 & 0 \\ 0 & 0 & 0 & 0 & 0 & 0 & 0 & A-8B & 0 & 0 \\ 0 & 0 & 0 & 0 & 0 & 0 & 0 & 0 & A-5B & -6B \\ 0 & 0 & 0 & 0 & 0 & 0 & 0 & 0 & -6B & A+4B \end{bmatrix} = U_T^t. \quad (C9)$$

Here, A , B , and C are the Racah parameters, given by combinations of the Slater integrals F_2 and F_4 ,

$$A = A_0 - \frac{49}{441}F_4, \quad B = \frac{1}{49}F_2 - \frac{5}{441}F_4, \quad C = \frac{35}{441}F_4. \quad (C10)$$

The parameter A_0 is determined such that upon diagonalizing simultaneously the Coulomb Hamiltonian and the crystal-field one, the lowest state has the energy U_{eff} as explained in Sec. IIB. Enumerating the singlets in the order

$$\begin{aligned}
|1\rangle &= \Psi_S^{55}, |2\rangle = \Psi_S^{22}, |3\rangle = \Psi_S^{33}, |4\rangle = \Psi_S^{44}, |5\rangle = \Psi_S^{11}, \\
|6\rangle &= \Psi_S^{52}, |7\rangle = \Psi_S^{51}, |8\rangle = \Psi_S^{34}, |9\rangle = \Psi_S^{21}, |10\rangle = \Psi_S^{41}, \\
|11\rangle &= \Psi_S^{53}, |12\rangle = \Psi_S^{23}, |13\rangle = \Psi_S^{13}, |14\rangle = \Psi_S^{54}, |15\rangle = \Psi_S^{24}, \quad (C11)
\end{aligned}$$

the Coulomb Hamiltonian in the singlet sector becomes

a. The Coulomb Hamiltonian

The Coulomb Hamiltonian, in the orthorhombic basis, is given by

$$H^c = \frac{1}{2} \sum_{\substack{k\sigma_1\sigma_2 \\ \gamma_1\gamma_2\gamma_3\gamma_4}} U_{\gamma_1\gamma_2\gamma_3\gamma_4} c_{k\gamma_1\sigma_1}^\dagger c_{k\gamma_2\sigma_2}^\dagger c_{k\gamma_3\sigma_2} c_{k\gamma_4\sigma_1}. \quad (C6)$$

In order to specify its matrix elements in the $3d^2$ sector (taken from Ref. 19) we construct the triplet ($\Psi_T^{\gamma\gamma'}$) and the singlet ($\Psi_S^{\gamma\gamma'}$) two-particle states in the orthorhombic basis,

$$\begin{aligned}
\Psi_T^{\gamma\gamma'}(k; \sigma\sigma') &= \sqrt{\frac{1}{2}} (c_{k\gamma\sigma}^\dagger c_{k\gamma'\sigma'}^\dagger + c_{k\gamma\sigma'}^\dagger c_{k\gamma\sigma}^\dagger) \\
&= -\Psi_T^{\gamma'\gamma}(k; \sigma\sigma'), \\
\Psi_S^{\gamma\gamma'}(k; \sigma\sigma') &= \sqrt{\frac{1}{2}} (c_{k\gamma\sigma}^\dagger c_{k\gamma'\sigma'}^\dagger - c_{k\gamma\sigma'}^\dagger c_{k\gamma\sigma}^\dagger) \\
&= \Psi_S^{\gamma'\gamma}(k; \sigma\sigma'), \\
\Psi_S^{\gamma\gamma}(k; \sigma\sigma') &= c_{k\gamma\sigma}^\dagger c_{k\gamma\sigma'}^\dagger. \quad (C7)
\end{aligned}$$

Altogether, there are 10 triplets and 15 singlets (in the $\sigma' = -\sigma$ sector). Enumerating the triplet states in the following order,

$$U_S = \begin{bmatrix} U_{S1} & 0 & 0 \\ 0 & U_{S2} & 0 \\ 0 & 0 & U_{S3} \end{bmatrix} = U_S^t, \quad (\text{C12})$$

where

$$U_{S1} = \begin{bmatrix} A+4B+3C & 4B+C & 3B+C & 3B+C & C & 0 \\ 4B+C & A+4B+3C & B+C & B+C & 4B+C & 0 \\ 3B+C & B+C & A+4B+3C & 3B+C & 3B+C & -B\sqrt{6} \\ 3B+C & B+C & 3B+C & A+4B+3C & 3B+C & B\sqrt{6} \\ C & 4B+C & 3B+C & 3B+C & A+4B+3C & 0 \\ 0 & 0 & -B\sqrt{6} & B\sqrt{6} & 0 & A+2C \end{bmatrix},$$

$$U_{S2} = \begin{bmatrix} A+4B+2C & 0 & 0 \\ 0 & A+B+2C & 2B\sqrt{3} \\ 0 & 2B\sqrt{3} & A+2C \end{bmatrix},$$

$$U_{S3} = \begin{bmatrix} A+B+2C & 3B & -B\sqrt{3} & 0 & 0 & 0 \\ 3B & A+B+2C & B\sqrt{3} & 0 & 0 & 0 \\ -B\sqrt{3} & B\sqrt{3} & A+3B+2C & 0 & 0 & 0 \\ 0 & 0 & 0 & A+B+2C & -3B & -B\sqrt{3} \\ 0 & 0 & 0 & -3B & A+B+2C & -B\sqrt{3} \\ 0 & 0 & 0 & -B\sqrt{3} & -B\sqrt{3} & A+3B+2C \end{bmatrix}. \quad (\text{C13})$$

b. The spin-orbit Hamiltonian

Written in the orthorhombic basis, the spin-orbit Hamiltonian is

$$H^{\text{so}} = \frac{\lambda}{2} \sum_{\substack{\alpha\gamma\gamma' \\ k\sigma\sigma'}} L_{\gamma\gamma'}^\alpha \sigma_{\sigma\sigma'}^\alpha c_{k\gamma\sigma}^\dagger c_{k\gamma'\sigma'}, \quad (\text{C14})$$

where α takes the values x, y , and z , σ^α are the Pauli matrices, and the angular momentum matrices $L_{\gamma\gamma'}^\alpha$ are

$$L^x = \begin{bmatrix} 0 & 0 & 0 & -i & 0 \\ 0 & 0 & i\sqrt{3} & 0 & 0 \\ 0 & -i\sqrt{3} & 0 & 0 & -i \\ i & 0 & 0 & 0 & 0 \\ 0 & 0 & i & 0 & 0 \end{bmatrix},$$

$$L^y = \begin{bmatrix} 0 & 0 & i & 0 & 0 \\ 0 & 0 & 0 & -i\sqrt{3} & 0 \\ -i & 0 & 0 & 0 & 0 \\ 0 & i\sqrt{3} & 0 & 0 & -i \\ 0 & 0 & 0 & i & 0 \end{bmatrix},$$

$$L^z = \begin{bmatrix} 0 & 0 & 0 & 0 & 2i \\ 0 & 0 & 0 & 0 & 0 \\ 0 & 0 & 0 & i & 0 \\ 0 & 0 & -i & 0 & 0 \\ -2i & 0 & 0 & 0 & 0 \end{bmatrix}. \quad (\text{C15})$$

Transformed into the crystal-field eigenstates, the spin-orbit Hamiltonian takes the form

$$H^{\text{so}} = \frac{\lambda}{2} \sum_{\substack{\alpha ii' \\ k\sigma\sigma'}} L_{ii'}^\alpha(k) \sigma_{\sigma\sigma'}^\alpha d_{ki\sigma}^\dagger d_{ki'\sigma'}, \quad (\text{C16})$$

with

$$L_{ii'}^\alpha(k) = \sum_{\gamma\gamma'} W_{i\gamma}(k) L_{\gamma\gamma'}^\alpha W_{\gamma'i'}^t(k). \quad (\text{C17})$$

Note that the relation $L_{\gamma\gamma'}^\alpha = -L_{\gamma'\gamma}^\alpha$ implies that $L_{ii'}^\alpha(k) = -L_{i'i}^\alpha(k)$.

c. The diagonalization of the two-electron states

When there are two electrons on the same Ti ion (at site k), their state is described by $d_{ki\sigma}^\dagger d_{kj\sigma'}^\dagger$. Using Eqs. (C3) and (C7), we re-write this state in terms of the singlet and triplet states,

$$\begin{aligned} d_{ki\sigma}^\dagger d_{kj\sigma'}^\dagger &= c_{k\gamma\sigma}^\dagger c_{k\gamma'\sigma'}^\dagger W_{i\gamma}(k) W_{j\gamma'}(k) \\ &= W_{i\gamma}(k) W_{j\gamma'}(k) \left\{ \Psi_S^{\gamma\gamma'}(k; \sigma\sigma') \delta_{\gamma\gamma'} \right. \\ &\quad \left. + \sqrt{\frac{1}{2}} \left[\Psi_T^{\gamma\gamma'}(k; \sigma\sigma') + \Psi_S^{\gamma\gamma'}(k; \sigma\sigma') \right] (1 - \delta_{\gamma\gamma'}) \right\}, \end{aligned} \quad (\text{C18})$$

where we have omitted for brevity the summation notations. Adopting the enumeration conventions Eqs. (C8) and (C11), this state can be cast conveniently into the form

$$d_{ki\sigma}^\dagger d_{kj\sigma'}^\dagger = \sum_{\mu=1}^{10} w_T^\mu(k; ij) \Psi_T^\mu(k; \sigma\sigma') + \sum_{\mu=1}^{15} w_S^\mu(k; ij) \Psi_S^\mu(k; \sigma\sigma'). \quad (C19)$$

Here we have introduced the 10-dimensional vector w_T , whose components are

$$w_T(k; ij) = \sqrt{\frac{1}{2}} \begin{bmatrix} W_{i5}(k)W_{j2}(k) - W_{i2}(k)W_{j5}(k), \\ W_{i5}(k)W_{j3}(k) - W_{i3}(k)W_{j5}(k), \\ W_{i4}(k)W_{j1}(k) - W_{i1}(k)W_{j4}(k), \\ W_{i2}(k)W_{j3}(k) - W_{i3}(k)W_{j2}(k), \\ W_{i5}(k)W_{j4}(k) - W_{i4}(k)W_{j5}(k), \\ W_{i1}(k)W_{j3}(k) - W_{i3}(k)W_{j1}(k), \\ W_{i2}(k)W_{j4}(k) - W_{i4}(k)W_{j2}(k), \\ W_{i2}(k)W_{j1}(k) - W_{i1}(k)W_{j2}(k), \\ W_{i3}(k)W_{j4}(k) - W_{i4}(k)W_{j3}(k), \\ W_{i5}(k)W_{j1}(k) - W_{i1}(k)W_{j5}(k) \end{bmatrix} \quad (C20)$$

and the 15-dimensional vector w_S ,

$$w_S(k; ij) = \begin{bmatrix} W_{i5}(k)W_{j5}(k), W_{i2}(k)W_{j2}(k), \\ W_{i3}(k)W_{j3}(k), W_{i4}(k)W_{j4}(k), \end{bmatrix}$$

$$W_{i1}(k)W_{j1}(k)], \quad (C21)$$

for the entries $\mu = 1, \dots, 5$, and

$$w_S(k; ij) = \sqrt{\frac{1}{2}} \begin{bmatrix} W_{i5}(k)W_{j2}(k) + W_{i2}(k)W_{j5}(k), \\ W_{i5}(k)W_{j1}(k) + W_{i1}(k)W_{j5}(k), \\ W_{i3}(k)W_{j4}(k) + W_{i4}(k)W_{j3}(k), \\ W_{i2}(k)W_{j1}(k) + W_{i1}(k)W_{j2}(k), \\ W_{i4}(k)W_{j1}(k) + W_{i1}(k)W_{j4}(k), \\ W_{i5}(k)W_{j3}(k) + W_{i3}(k)W_{j5}(k), \\ W_{i2}(k)W_{j3}(k) + W_{i3}(k)W_{j2}(k), \\ W_{i3}(k)W_{j1}(k) + W_{i1}(k)W_{j3}(k), \\ W_{i5}(k)W_{j4}(k) + W_{i4}(k)W_{j5}(k), \\ W_{i2}(k)W_{j4}(k) + W_{i4}(k)W_{j2}(k) \end{bmatrix}, \quad (C22)$$

for the entries $\mu = 6, \dots, 15$.

In order to obtain the two-states energies, we need to diagonalize simultaneously the Coulomb Hamiltonian and the crystal-field one. We have already written the Coulomb Hamiltonian matrix in terms of the triplets and the singlets. The next step is to express the crystal-field Hamiltonian in terms of those. Omitting for brevity the site index k , the crystal-field Hamiltonian matrix in the triplet sector is

$$V_T = \begin{bmatrix} V_{22}+V_{55} & V_{23} & 0 & -V_{35} & V_{24} & 0 & -V_{45} & -V_{15} & 0 & V_{12} \\ V_{23} & V_{33}+V_{55} & 0 & V_{25} & V_{34} & V_{15} & 0 & 0 & -V_{45} & V_{13} \\ 0 & 0 & V_{11}+V_{44} & 0 & -V_{15} & -V_{34} & -V_{12} & V_{24} & -V_{13} & V_{45} \\ -V_{35} & V_{25} & 0 & V_{22}+V_{33} & 0 & V_{12} & V_{34} & V_{13} & -V_{24} & 0 \\ V_{24} & V_{34} & -V_{15} & 0 & V_{44}+V_{55} & 0 & V_{25} & 0 & V_{35} & V_{14} \\ 0 & V_{15} & -V_{34} & V_{12} & 0 & V_{11}+V_{33} & 0 & -V_{23} & -V_{14} & -V_{35} \\ -V_{45} & 0 & -V_{12} & V_{34} & V_{25} & 0 & V_{22}+V_{44} & V_{14} & V_{23} & 0 \\ -V_{15} & 0 & V_{24} & V_{13} & 0 & -V_{23} & V_{14} & V_{11}+V_{22} & 0 & V_{25} \\ 0 & -V_{45} & -V_{13} & -V_{24} & V_{35} & -V_{14} & V_{23} & 0 & V_{33}+V_{44} & 0 \\ V_{12} & V_{13} & V_{45} & 0 & V_{14} & -V_{35} & 0 & V_{25} & 0 & V_{11}+V_{55} \end{bmatrix} = V_T^t. \quad (C23)$$

We are now in position to find the resolvent operator in the triplet sector. Denoting by B the (unitary and real) matrix that diagonalizes the triplet part of $H^{\text{cf}} + H^c$, and by E_T^μ the corresponding eigenenergies, we have

$$\frac{1}{\Delta\mathcal{E}} \Psi_T^\mu(k; \sigma\sigma') = - \sum_{\mu'} X_T^k(\mu, \mu') \Psi_T^{\mu'}(k; \sigma\sigma'), \quad (C24)$$

where $1/\Delta\mathcal{E}$ is the resolvent operator²⁴ and

$$X_T^k(\mu, \mu') = - \sum_{\mu_1=1}^{10} \frac{B_k(\mu, \mu_1) B_k^t(\mu_1, \mu')}{E_T^{\mu_1}}. \quad (C25)$$

One notes that since $B_k(\mu, \mu') = B_k^t(\mu', \mu)$, the matrices X_T^k satisfy

$$X_T^k(\mu, \mu') = X_T^k(\mu', \mu). \quad (C26)$$

Turning now to the singlet sector, we first find the crystal-field Hamiltonian matrix of the singlets,

$$V_S = \begin{bmatrix} V_{S1} & V_{S2} & V_{S3} \\ V_{S2}^t & V_{S4} & V_{S5} \\ V_{S3}^t & V_{S5}^t & V_{S6} \end{bmatrix} = V_S^t, \quad (C27)$$

where

$$\begin{aligned}
V_{S1} &= \begin{bmatrix} 2V_{55} & 0 & 0 & 0 & 0 & \sqrt{2}V_{25} \\ 0 & 2V_{22} & 0 & 0 & 0 & \sqrt{2}V_{25} \\ 0 & 0 & 2V_{33} & 0 & 0 & 0 \\ 0 & 0 & 0 & 2V_{44} & 0 & 0 \\ 0 & 0 & 0 & 0 & 2V_{11} & 0 \\ \sqrt{2}V_{25} & \sqrt{2}V_{25} & 0 & 0 & 0 & V_{22} + V_{55} \end{bmatrix}, & V_{S2} &= \begin{bmatrix} \sqrt{2}V_{15} & 0 & 0 \\ 0 & 0 & \sqrt{2}V_{12} \\ 0 & \sqrt{2}V_{34} & 0 \\ 0 & \sqrt{2}V_{34} & 0 \\ \sqrt{2}V_{15} & 0 & \sqrt{2}V_{12} \\ V_{12} & 0 & V_{15} \end{bmatrix}, \\
V_{S3} &= \begin{bmatrix} 0 & \sqrt{2}V_{35} & 0 & 0 & \sqrt{2}V_{45} & 0 \\ 0 & 0 & \sqrt{2}V_{23} & 0 & 0 & \sqrt{2}V_{24} \\ 0 & \sqrt{2}V_{35} & \sqrt{2}V_{23} & \sqrt{2}V_{13} & 0 & 0 \\ \sqrt{2}V_{15} & 0 & 0 & 0 & \sqrt{2}V_{45} & \sqrt{2}V_{24} \\ \sqrt{2}V_{14} & 0 & 0 & \sqrt{2}V_{13} & 0 & 0 \\ 0 & V_{23} & V_{35} & 0 & V_{24} & V_{45} \end{bmatrix}, \\
V_{S4} &= \begin{bmatrix} V_{11} + V_{55} & 0 & V_{25} \\ 0 & V_{33} + V_{44} & 0 \\ V_{25} & 0 & V_{11} + V_{22} \end{bmatrix}, & V_{S5} &= \begin{bmatrix} V_{45} & V_{13} & 0 & V_{35} & V_{14} & 0 \\ V_{13} & V_{45} & V_{24} & V_{14} & V_{35} & V_{23} \\ V_{24} & 0 & V_{13} & V_{23} & 0 & V_{14} \end{bmatrix}, \\
V_{S6} &= \begin{bmatrix} V_{11} + V_{44} & 0 & 0 & V_{34} & V_{15} & V_{12} \\ 0 & V_{33} + V_{55} & V_{25} & V_{15} & V_{34} & 0 \\ 0 & V_{25} & V_{22} + V_{33} & V_{12} & 0 & V_{34} \\ V_{34} & V_{15} & V_{12} & V_{11} + V_{33} & 0 & 0 \\ V_{15} & V_{34} & 0 & 0 & V_{44} + V_{55} & V_{25} \\ V_{12} & 0 & V_{34} & 0 & V_{25} & V_{22} + V_{44} \end{bmatrix}. \tag{C28}
\end{aligned}$$

Then we introduce the (15×15) matrix C that diagonalizes $H^{\text{cf}} + H^c$ of the singlets and the corresponding eigenenergies E_S^μ . Analogously to Eq. (C25), it is convenient here to define as well

$$X_S^k(\mu, \mu') = - \sum_{\mu_1=1}^{15} \frac{C_k(\mu, \mu_1) C_k^t(\mu_1, \mu')}{E_S^{\mu_1}}, \tag{C29}$$

which satisfies

$$X_S^k(\mu, \mu') = X_S^k(\mu', \mu). \tag{C30}$$

Analogously to Eq. (C24) we have

$$\frac{1}{\Delta \mathcal{E}} \Psi_S^\mu(k; \sigma \sigma') = - \sum_{\mu'} X_S^k(\mu, \mu') \Psi_S^{\mu'}(k; \sigma \sigma'). \tag{C31}$$

Collecting the results above, the intermediate two-particle states of the perturbation expansion are now given in the form

$$\begin{aligned}
& \frac{1}{\Delta \mathcal{E}} d_{ki\sigma}^\dagger d_{kj\sigma'}^\dagger \\
&= \sum_{\mu\mu'=1}^{10} w_T^\mu(k; ij) X_T^k(\mu, \mu') \Psi_T^{\mu'}(k; \sigma \sigma') \\
&+ \sum_{\mu\mu'=1}^{15} w_S^\mu(k; ij) X_S^k(\mu, \mu') \Psi_S^{\mu'}(k; \sigma \sigma'). \tag{C32}
\end{aligned}$$

The final step involves transforming back Ψ_T and Ψ_S into the d operators. Consider, for example, $\Psi_T^{\mu'}$ with $\mu' = \gamma_1 \gamma_2$. Using Eqs. (C3) and (C7), we find (omitting the summation notations for brevity)

$$\begin{aligned}
& \Psi_T^{\gamma_1 \gamma_2}(k; \sigma \sigma') \\
&= \sqrt{\frac{1}{2}} W_{i_1 \gamma_1}(k) W_{i_2 \gamma_2}(k) \\
&\quad \times \left(d_{ki_1 \sigma}^\dagger d_{ki_2 \sigma'}^\dagger + d_{ki_1 \sigma'}^\dagger d_{ki_2 \sigma}^\dagger \right) \\
&= d_{ki_1 \sigma}^\dagger d_{ki_2 \sigma'}^\dagger \\
&\quad \times \sqrt{\frac{1}{2}} \left[W_{i_1 \gamma_1}(k) W_{i_2 \gamma_2}(k) - W_{i_2 \gamma_1}(k) W_{i_1 \gamma_2}(k) \right] \\
&= d_{ki_1 \sigma}^\dagger d_{ki_2 \sigma'}^\dagger w_T^{\mu'}(k; i_1 i_2). \tag{C33}
\end{aligned}$$

A similar calculation holds for the singlets. We therefore may write

$$\frac{1}{\Delta \mathcal{E}} d_{ki\sigma}^\dagger d_{ki'\sigma'}^\dagger = Z_k(ii'; i_1 i_2) d_{ki_1 \sigma}^\dagger d_{ki_2 \sigma'}^\dagger, \tag{C34}$$

with

$$\begin{aligned}
Z_k(ii'; i_1 i_2) &= \sum_{\mu\mu'=1}^{10} w_T^\mu(k; ii') X_T^k(\mu, \mu') w_T^{\mu'}(k; i_1 i_2) \\
&+ \sum_{\mu\mu'=1}^{15} w_S^\mu(k; ii') X_S^k(\mu, \mu') w_S^{\mu'}(k; i_1 i_2).
\end{aligned}$$

$$(C35) \quad \frac{1}{\Delta\mathcal{E}} P_{mn}^1 = - \sum_{\substack{\sigma\sigma' \\ i_1 i_2 (\neq 00)}} \frac{1}{E_{i_1} + E_{i_2}} d_{mi_1\sigma}^\dagger d_{ni_2\sigma'}^\dagger |0\rangle \langle 0| d_{ni_2\sigma'} d_{mi_1\sigma}. \quad (C40)$$

We note that since the X 's are symmetric, it follows that

$$Z_k(ii'; i_1 i_2) = Z_k(i_1 i_2; ii'). \quad (C36)$$

Also, since $w_S^\mu(k; ii') = w_S^\mu(k; i'i)$ and $w_T^\mu(k; ii') = -w_T^\mu(k; i'i)$, one has

$$Z_k(ii'; i_1 i_2) = Z_k(i'i; i_2 i_1). \quad (C37)$$

2. Perturbation expansion

Our formal expressions of the various terms in the perturbation expansion, Eqs. (19), (20), and (21) above, involve the projection operators P_{mn}^0 and $S_{mn} = (1 - P_{mn}^0)/\Delta\mathcal{E}$. Here we give their explicit expressions in terms of the quantities derived in the first part of this Appendix.

The projector onto the unperturbed ground-state space is

$$P_{mn}^0 = \sum_{\sigma\sigma'} d_{m0\sigma}^\dagger d_{n0\sigma'}^\dagger |0\rangle \langle 0| d_{n0\sigma'} d_{m0\sigma}, \quad (C38)$$

where $|0\rangle$ denotes the vacuum state. Similarly, the projector onto the Ti^{3+} sector of the excited states is

$$P_{mn}^1 = \sum_{\substack{\sigma\sigma' \\ i_1 i_2 (\neq 00)}} d_{mi_1\sigma}^\dagger d_{ni_2\sigma'}^\dagger |0\rangle \langle 0| d_{ni_2\sigma'} d_{mi_1\sigma}. \quad (C39)$$

It follows that the resolvent operator applied to P_{mn}^1 is given by

a. The Heisenberg couplings. These are given by

$$J_{mn} = - \sum_{i_1 i_2} [t_{mn}^{i_1 0} Z_m(i_1 0; 0 i_2) t_{nm}^{0 i_2} + t_{nm}^{i_1 0} Z_n(i_1 0; 0 i_2) t_{mn}^{0 i_2}]. \quad (C44)$$

b. The Moriya vectors. These are given to first order in the spin-orbit coupling,

$$D_{mn}^\alpha = 2i\lambda \sum_{\substack{i(\neq 0) \\ i_1 i_2}} \frac{1}{E_i} \{ L_{i0}^\alpha(m) [t_{mn}^{i_1 0} Z_m(i_1 i; 0 i_2) t_{nm}^{0 i_2} + t_{nm}^{i_1 i} Z_n(i_1 0; 0 i_2) t_{mn}^{0 i_2}] \\ - L_{i0}^\alpha(n) [t_{mn}^{i_1 0} Z_m(i_1 0; 0 i_2) t_{nm}^{i i_2} + t_{nm}^{i_1 0} Z_n(i_1 0; i i_2) t_{mn}^{0 i_2}] \}. \quad (C45)$$

c. The symmetric anisotropies, and the λ^2 correction of the Moriya vectors. These terms are of second order in λ , and have a more complicated structure. In order to present them in a concised fashion, we write the left-hand-side of Eq. (21) in the form

$$\mathbf{S}_m A_{mn}^s \mathbf{S}_n + \mathbf{D}'_{mn} (\mathbf{S}_m \times \mathbf{S}_n) = J'_{mn} \mathbf{S}_m \mathbf{S}_n + \sum_{\substack{\alpha\beta l \\ i(\neq 0) \\ i'(\neq 0)}} \frac{1}{E_i E_{i'}} C_{mn}^{\alpha\beta}(i, i', l) I_{mn}^{\alpha\beta}(l), \quad (C46)$$

where J'_{mn} and \mathbf{D}'_{mn} are the λ^2 corrections of the Heisenberg couplings and the Moriya vectors, respectively. In Eq. (C46) l enumerates the 4 spin invariants, such that

In a similar way, the projector onto the Ti^{2+} sector of the excited states is

$$P_{mn}^2 = \frac{1}{2} \sum_{k\sigma\sigma'} \left[\sum_{\mu=1}^{10} \Psi_T^\mu(k; \sigma\sigma') |0\rangle \langle 0| \Psi_T^{\mu\dagger}(k; \sigma\sigma') \right. \\ \left. + \sum_{\mu=1}^{15} \Psi_S^\mu(k; \sigma\sigma') |0\rangle \langle 0| \Psi_S^{\mu\dagger}(k; \sigma\sigma') \right], \quad (C41)$$

which gives, upon applying the resolvent operator,

$$\frac{1}{\Delta\mathcal{E}} P_{mn}^2 = - \frac{1}{2} \sum_{k\sigma\sigma'} \left[\sum_{\mu\mu'} X_T^k(\mu, \mu') \Psi_T^{\mu'}(k; \sigma\sigma') |0\rangle \right. \\ \times \langle 0| \Psi_T^{\mu\dagger}(k; \sigma\sigma') \\ \left. + \sum_{\mu\mu'} X_S^k(\mu, \mu') \Psi_S^{\mu'}(k; \sigma\sigma') |0\rangle \right. \\ \times \langle 0| \Psi_S^{\mu\dagger}(k; \sigma\sigma') \left. \right]. \quad (C42)$$

Hence, the combined resolvent and projection operator onto the excited states is

$$S_{mn} = \frac{1}{\Delta\mathcal{E}} (P_{mn}^1 + P_{mn}^2). \quad (C43)$$

Collecting these results, and expressing the products of d in terms of the ground-state spin operators [see Eqs. (15)], one obtains the magnetic exchange couplings. These are listed below.

$$\begin{aligned}
I_{mn}^{\alpha\beta}(1) &= S_m^\alpha S_n^\beta, \quad I_{mn}^{\alpha\beta}(2) = S_m^\alpha S_n^\beta + S_m^\beta S_n^\alpha - \delta_{\alpha\beta} \mathbf{S}_m \cdot \mathbf{S}_n, \\
I_{mn}^{\alpha\beta}(3) &= \delta_{\alpha\beta} \mathbf{S}_m \cdot \mathbf{S}_n + \sum_{\gamma} \epsilon_{\alpha\beta\gamma} (\mathbf{S}_m \times \mathbf{S}_n)^\gamma, \quad I_{mn}^{\alpha\beta}(4) = I_{mn}^{\beta\alpha}(3),
\end{aligned} \tag{C47}$$

where $\epsilon_{\alpha\beta\gamma}$ is the totally antisymmetric tensor. It remains to list the coefficients appearing in Eq. (C46). These are given by

$$\begin{aligned}
J'_{mn} &= -J_{mn} \frac{\lambda^2}{4} \sum_{\substack{\alpha \\ i(\neq 0)}} \frac{1}{E_i^2} [|L_{i0}^\alpha(m)|^2 + |L_{i0}^\alpha(n)|^2], \\
C_{mn}^{\alpha\beta}(i, i', 1) &= 2\lambda^2 \sum_{i_1 i_2} L_{i0}^\alpha(m) L_{0i'}^\beta(n) [t_{mn}^{i_1 0} Z_m(i i_1; 0 i_2) t_{nm}^{i' i_2} + t_{nm}^{i_1 0} Z_n(i' i_1; 0 i_2) t_{mn}^{i i_2} \\
&\quad - t_{mn}^{i_1 0} Z_m(i_1 0; i_2 i) t_{nm}^{i' i_2} - t_{nm}^{i_1 0} Z_n(i_1 0; i_2 i') t_{mn}^{i i_2}], \\
C_{mn}^{\alpha\beta}(i, i', 2) &= -\lambda^2 \sum_{i_1 i_2} \left\{ \frac{1}{2} L_{i0}^\alpha(m) L_{0i'}^\beta(m) [t_{mn}^{i_1 0} Z_m(i' i_1; i_2 i) t_{nm}^{0 i_2} + t_{nm}^{i_1 i'} Z_n(i_1 0; 0 i_2) t_{mn}^{i i_2}] \right. \\
&\quad + \frac{1}{2} L_{i0}^\alpha(n) L_{0i'}^\beta(n) [t_{mn}^{i_1 i} Z_m(i_1 0; 0 i_2) t_{nm}^{i' i_2} + t_{nm}^{i_1 0} Z_n(i i_1; i_2 i') t_{mn}^{0 i_2}] \\
&\quad \left. - L_{i0}^\alpha(m) L_{0i'}^\beta(n) [t_{mn}^{i_1 0} Z_m(i_1 0; i i_2) t_{nm}^{i' i_2} + t_{nm}^{i_1 0} Z_n(i_1 0; i' i_2) t_{mn}^{i i_2}] \right\}, \\
C_{mn}^{\alpha\beta}(i, i', 3) &= -\lambda^2 \sum_{i_1 i_2} \left\{ \frac{1}{2} L_{i0}^\alpha(m) L_{0i'}^\beta(n) [t_{mn}^{i_1 i'} Z_m(i_1 0; i i_2) t_{nm}^{0 i_2} + t_{nm}^{i_1 0} Z_n(i' i_1; i_2 0) t_{mn}^{i i_2}] \right. \\
&\quad \left. + L_{i0}^\alpha(m) L_{i'i}^\beta(m) [t_{mn}^{i_1 0} Z_m(i_1 0; i' i_2) t_{nm}^{0 i_2} + t_{nm}^{i_1 0} Z_n(i_1 0; 0 i_2) t_{mn}^{i' i_2}] \right\}, \\
C_{mn}^{\alpha\beta}(i, i', 4) &= -\lambda^2 \sum_{i_1 i_2} \left\{ \frac{1}{2} L_{i0}^\beta(m) L_{0i'}^\alpha(n) [t_{mn}^{i_1 i'} Z_m(i_1 0; i i_2) t_{nm}^{0 i_2} + t_{nm}^{i_1 0} Z_n(i' i_1; i_2 0) t_{mn}^{i i_2}] \right. \\
&\quad \left. + L_{i0}^\alpha(n) L_{i'i}^\beta(n) [t_{mn}^{i_1 0} Z_m(i_1 0; 0 i_2) t_{nm}^{i' i_2} + t_{nm}^{i_1 0} Z_n(i_1 0; i' i_2) t_{mn}^{0 i_2}] \right\}. \tag{C48}
\end{aligned}$$

TABLE I. The parametrization of the unit cell (space group $Pbnm$), modulo the lattice constants a, b, c .

La	$(x_{\text{RE}}, y_{\text{RE}}, 1/4), (1/2 - x_{\text{RE}}, 1/2 + y_{\text{RE}}, 1/4),$ $(-x_{\text{RE}}, -y_{\text{RE}}, 3/4), (1/2 + x_{\text{RE}}, 1/2 - y_{\text{RE}}, 3/4)$
Ti	$(0, 1/2, 0), (1/2, 0, 0), (0, 1/2, 1/2), (1/2, 0, 1/2)$
O1	$(x_{\text{O1}}, y_{\text{O1}}, 1/4), (1/2 - x_{\text{O1}}, 1/2 + y_{\text{O1}}, 1/4),$ $(-x_{\text{O1}}, -y_{\text{O1}}, 3/4), (1/2 + x_{\text{O1}}, 1/2 - y_{\text{O1}}, 3/4)$
O2	$(x_{\text{O2}}, y_{\text{O2}}, z_{\text{O2}}), (x_{\text{O2}}, y_{\text{O2}}, 1/2 - z_{\text{O2}}),$ $(-x_{\text{O2}}, -y_{\text{O2}}, -z_{\text{O2}}), (-x_{\text{O2}}, -y_{\text{O2}}, 1/2 + z_{\text{O2}}),$ $(1/2 - x_{\text{O2}}, 1/2 + y_{\text{O2}}, z_{\text{O2}}),$ $(1/2 - x_{\text{O2}}, 1/2 + y_{\text{O2}}, 1/2 - z_{\text{O2}}),$ $(1/2 + x_{\text{O2}}, 1/2 - y_{\text{O2}}, -z_{\text{O2}}),$ $(1/2 + x_{\text{O2}}, 1/2 - y_{\text{O2}}, 1/2 + z_{\text{O2}})$

TABLE II. The symmetries of the space group $Pbnm$.

Inversion centers	Ti sites and centers of ab -planar Ti plaquettes, i. e. $(0, 0, 0), (1/2, 1/2, 0)$, etc.
Mirror planes	$z = \pm 1/4$
Glide planes	$x = \pm 1/4$, translation by $(0, 1/2, 0)$
Screw axes	Through the inversion centers, along the z axis, rotation by 180°

TABLE III. The static crystal field for Ti^{3+} (site 1): Spectrum and eigenstates in the orthorhombic basis for the d orbitals, see Eq. (1) and the following comment there. [The eigenenergies E_i and the matrix $W(1)$ used in conjunction with Eq. (C4) are defined by the spectrum and the coordinates of the eigenstates, respectively, as given in this Table, where the first row of $W(1)$ is the coordinate vector of the ground state, etc.]

-0.468 eV	$(-0.035, \quad 0.016, \quad 0.770, \quad -0.035, \quad 0.636)$
-0.259 eV	$(-0.052, \quad -0.397, \quad 0.088, \quad 0.911, \quad -0.049)$
-0.239 eV	$(-0.407, \quad 0.035, \quad -0.587, \quad 0.086, \quad 0.693)$
0.452 eV	$(0.853, \quad 0.315, \quad -0.197, \quad 0.221, \quad 0.290)$
0.515 eV	$(-0.319, \quad 0.861, \quad 0.123, \quad 0.336, \quad -0.169)$
Basis	$ xy\rangle, \quad 2z^2\rangle, \quad yz\rangle, \quad xz\rangle, \quad x^2 - y^2\rangle$

TABLE IV. The effective Ti–Ti hopping matrices for the d eigen-orbitals of the crystal field from Table III; values are given in eV. The rows and the columns are ordered beginning with the ground state of the crystal field (index 0), continuing with the first excited state (index 1), etc. t_{13} is symmetric due to the mirror plane at $z = 1/4$. As the matrices are given in terms of the crystal-field eigen-basis, the dependence of the hopping matrices on the bonds is particularly simple. [In contrast, had we used the orthorhombic basis (1), additional minus signs would have appeared in several entries.]

Planar					
$t_{12} = t_{16}^t = t_{25} = t_{65}^t = t_{34} = t_{38}^t = t_{47} = t_{87}^t$					
=	$\begin{bmatrix} -0.198 & -0.155 & -0.052 & -0.022 & 0.016 \\ 0.109 & 0.133 & 0.022 & -0.089 & 0.135 \\ -0.114 & 0.167 & -0.188 & -0.098 & 0.193 \\ -0.021 & 0.088 & -0.235 & 0.579 & -0.710 \\ 0.010 & -0.019 & -0.003 & 0.089 & -0.121 \end{bmatrix}$				
Inter-planar					
$t_{13} = t_{24} = t_{39} = t_{410}$					
=	$\begin{bmatrix} 0.178 & 0.047 & -0.143 & 0.010 & 0.020 \\ 0.047 & 0.244 & 0.072 & 0.135 & 0.224 \\ -0.143 & 0.072 & 0.146 & -0.008 & -0.057 \\ 0.010 & 0.135 & -0.008 & -0.112 & -0.312 \\ 0.020 & 0.224 & -0.057 & -0.312 & -0.812 \end{bmatrix}$				

TABLE V. Model parameters of the calculation.

Momenta of the effective ionic radius for Ti^{3+}	
$\langle r^2 \rangle = 0.530 \text{ \AA}^2$, $\langle r^4 \rangle = 0.554 \text{ \AA}^4$	
Slater integrals for Ti^{2+}	
$F_2 = 8F_4/5 = 8.3 \text{ eV}$	
Spin-orbit parameter	
$\lambda = 18 \text{ meV}$	
Slater-Koster parameters	
$V_{pd\sigma} = -2.4 \text{ eV}$, $V_{pd\pi} = 1.3 \text{ eV}$	
Effective charge-transfer energies (Ti–Ti, Ti–O)	
$U_{\text{eff}} = 3.5 \text{ eV}$, $\Delta_{\text{eff}} = 5.5 \text{ eV}$	

TABLE VI. The combined static and covalent crystal fields for Ti^{3+} (site 1): Spectrum and eigenstates in the orthorhombic basis for the d orbitals. The covalent contribution is calculated for a TiO_6 cluster. The full eigenstates are linear combinations of Ti^{3+} states and Ti^{2+} states (accompanied by a p hole on one of the oxygen sites). Here, only the Ti^{3+} parts of the five lowest eigenstates are shown, corresponding to the states $|d^1\rangle$ of Eq. (13).

–0.663 eV	$(-0.029, 0.020, 0.778, -0.023, 0.627)$
–0.441 eV	$(0.084, -0.383, 0.200, 0.875, -0.200)$
–0.430 eV	$(-0.393, -0.089, -0.550, 0.279, 0.676)$
0.737 eV	$(0.856, 0.322, -0.211, 0.173, 0.297)$
0.797 eV	$(-0.323, 0.861, 0.092, 0.354, -0.144)$
Basis	$ xy\rangle, 2z^2\rangle, yz\rangle, xz\rangle, x^2-y^2\rangle$

TABLE VII. Symmetries of the effective spin Hamiltonian due to the space group. The relations among the anisotropic couplings are abbreviated as follows. $(+, +, +)_{12} = (-, +, +)_{16}$ means $\mathbf{D}_{12} = (-D_{16}^x, D_{16}^y, D_{16}^z)$, etc. Due to the mirror plane $z = 1/4$, the inter-plane Moriya vectors have vanishing z components and the inter-plane symmetric anisotropies have vanishing yz and xz entries. The transformation of the symmetric anisotropies is characterized by the off-diagonal coefficients ($A_{mn}^{yz}, A_{mn}^{xz}, A_{mn}^{xy}$) whereas the diagonal coefficients are invariant in and between the planes, respectively.

Heisenberg couplings	
$J_{12} = J_{16} = J_{25} = J_{65} = J_{34} = J_{38} = J_{47} = J_{87}$,	
$J_{13} = J_{24} = J_{39} = J_{410}$	
Moriya vectors	
$(+, +, +)_{12} = (-, +, +)_{16} = (+, -, -)_{25} = (-, -, -)_{65}$	
$= (-, -, +)_{34} = (+, -, +)_{38} = (-, +, -)_{47} = (+, +, -)_{87}$,	
$(+, +, 0)_{13} = (+, -, 0)_{24} = (-, -, 0)_{39} = (-, +, 0)_{410}$	
Symmetric anisotropies	
$(+, +, +)_{12} = (+, -, -)_{16} = (+, -, -)_{25} = (+, +, +)_{65}$	
$= (-, -, +)_{34} = (-, +, -)_{38} = (-, +, -)_{47} = (-, -, +)_{87}$,	
$(0, 0, +)_{13} = (0, 0, -)_{24} = (0, 0, +)_{39} = (0, 0, -)_{410}$	

TABLE VIII. The calculated single-bond spin couplings (in meV). The Moriya vectors are given including the corrections \mathbf{D}'_{mn} , which are of order λ^2 . The symmetric anisotropies are given as $\mathbf{A}_{mn}^d = (A_{mn}^{xx}, A_{mn}^{yy}, A_{mn}^{zz})$ and $\mathbf{A}_{mn}^{od} = (A_{mn}^{yz}, A_{mn}^{xz}, A_{mn}^{xy})$ for the diagonal and off-diagonal entries, respectively.

Heisenberg couplings	
$J_{12} = 24.616, J_{13} = 19.416$	
Moriya vectors	
$\mathbf{D}_{12} = (3.254, -1.273, -1.286), \mathbf{D}_{13} = (-2.886, 0.543, 0)$	
Symmetric anisotropies	
$\mathbf{A}_{12}^d = (0.188, 0.066, 0.037), \mathbf{A}_{13}^d = (-0.039, -0.218, -0.190),$ $\mathbf{A}_{12}^{od} = (-0.035, -0.111, -0.088), \mathbf{A}_{13}^{od} = (0, 0, -0.074)$	

TABLE IX. The macroscopic couplings of the sublattice magnetizations in terms of the microscopic single-bond spin couplings. For instance, we have $I_{12} = J_{12}$ but $I_{13} = J_{13}/2$. This is because the coordination number of a Ti ion is 4 in the planes and 2 between the planes.

Isotropic couplings	
$I_{12} = J_{12}, I_{13} = \frac{1}{2}J_{13}$	
Dzyaloshinskii vectors	
$\mathbf{D}_{12}^D = (0, D_{12}^y, D_{12}^z), \mathbf{D}_{13}^D = \frac{1}{2}\mathbf{D}_{13}$	
Macroscopic symmetric anisotropies	
$\Gamma_{12}^d = \mathbf{A}_{12}^d, \Gamma_{12}^{od} = (A_{12}^{yz}, 0, 0), \Gamma_{13} = \frac{1}{2}A_{13}$	

TABLE X. Symmetries of the magnetic Hamiltonian due to the space group. The relations for the anisotropic couplings are abbreviated as in Table VII. Due to the glide planes, the Dzyaloshinskii vectors of the planar bonds have vanishing x components, and the respective symmetric anisotropies have vanishing xz and xy entries. Because of the mirror planes, the Dzyaloshinskii vectors of the inter-planar bonds have vanishing z components and the respective symmetric anisotropies have vanishing yz and xz entries.

Isotropic couplings	
$I_{12} = I_{34}, I_{13} = I_{24}$	
Dzyaloshinskii vectors	
$(0, +, +)_{12} = (0, -, +)_{34}, (+, +, 0)_{13} = (+, -, 0)_{24}$	
Macroscopic symmetric anisotropies	
$(+, 0, 0)_{12} = (-, 0, 0)_{34}, (0, 0, +)_{13} = (0, 0, -)_{24}$	

TABLE XI. All types of magnetic order which are allowed by the space group $Pbnm$. There are four possibilities, denoted by x^s, x^a, z^s , and z^a . They are allowed because the ordered state can be symmetric or antisymmetric according to the glide plane $x = 1/4$ and the mirror plane $z = 1/4$, respectively. The order in LaTiO_3 is of the first type. Here, G_x denotes G-type antiferromagnetic moment along x , A_y denotes A-type antiferromagnetic moment along y , and F_z denotes ferromagnetic moment along z . The other possibilities involve also C-type ordering, e.g. C_z for the z components of the magnetic moments. The magnetizations \mathbf{M}_k of the sublattices are given in terms of \mathbf{M}_1 . $(+, +, +)_1 = (-, +, +)_2$ means $\mathbf{M}_1 = (-M_2^x, M_2^y, M_2^z)$, etc.

1. x^s, z^a	2. x^a, z^a	3. x^s, z^s	4. x^a, z^s
$(+, +, +)_1$	$(+, +, +)_1$	$(+, +, +)_1$	$(+, +, +)_1$
$=(-, +, +)_2$	$=(+, -, -)_2$	$=(-, +, +)_2$	$=(+, -, -)_2$
$=(-, -, +)_3$	$=(-, -, +)_3$	$=(+, +, -)_3$	$=(+, +, -)_3$
$=(+, -, +)_4$	$=(-, +, -)_4$	$=(-, +, -)_4$	$=(+, -, +)_4$
$G_x A_y F_z$	$A_x G_y C_z$	$C_x F_y A_z$	$F_x C_y G_z$

TABLE XII. The structure of the magnetic order (the first possibility of Table XI), characterized by the sublattice magnetizations \mathbf{M}_k in the classical ground state, in terms of the canting angles φ and ϑ . Each of these angles is proportional to λ , the spin-orbit parameter.

x components: G-type
$-M_1^x = M_2^x = M_3^x = -M_4^x = \cos \varphi \cos \vartheta$
y components: A-type
$-M_1^y = -M_2^y = M_3^y = M_4^y = \sin \varphi \cos \vartheta$
z components: ferromagnetic
$M_1^z = M_2^z = M_3^z = M_4^z = \sin \vartheta$

TABLE XIII. The values of the macroscopic magnetic couplings in meV, the resulting canting angles of the magnetizations in the classical ground state, and the resulting absolute values of the ordered moments (normalized to $1 \mu_B$, i.e., without the reduction due to quantum fluctuations and the spin-orbit coupling). The three coefficients of the macroscopic symmetric anisotropies are taken into account (see text).

Isotropic couplings
$I_{12} = 24.616, I_{13} = 9.708$
Dzyaloshinskii vectors
$\mathbf{D}_{12}^D = (0, -1.273, -1.286), \mathbf{D}_{13}^D = (-1.589, 0.271, 0)$
Macroscopic symmetric anisotropies
$\Gamma_{12}^{xx} = 0.188, \Gamma_{13}^{xx} = -0.020, \Gamma_{13}^{xy} = -0.037$
Canting angles
$\varphi = 1.42^\circ, \vartheta = 0.80^\circ$
Ordered moments
$\mathbf{M} = (0.9996, 0.0248, 0.0140) \mu_B$

-
- ¹ M. Imada *et al.*, Rev. Mod. Phys. **70**, 1039 (1998).
² G. I. Meijer *et al.*, Phys. Rev. B **59**, 11832 (1999).
³ G. Khaliullin and S. Maekawa, Phys. Rev. Lett. **85**, 3950 (2000).
⁴ M. Cwik *et al.*, Phys. Rev. B **68**, 060401 (2003).
⁵ M. Haverkort *et al.*, cond-mat/0405516 (2004).
⁶ B. Keimer *et al.*, Phys. Rev. Lett. **85**, 3946 (2000).
⁷ E. Pavarini *et al.*, Phys. Rev. Lett. **92**, 176403 (2004).
⁸ I. V. Solovyev, Phys. Rev. B **69**, 134403 (2004).
⁹ T. Kiyama and M. Itoh, Phys. Rev. Lett. **91**, 167202 (2003).
¹⁰ P. Lunkenheimer *et al.*, Phys. Rev. B **68**, 245108 (2003).
¹¹ V. Fritsch *et al.*, Phys. Rev. B **65**, 212405 (2002).
¹² A. B. Harris *et al.*, Phys. Rev. Lett. **91**, 087206 (2003).
¹³ A. B. Harris *et al.*, Phys. Rev. B **69**, 035107 (2004).
¹⁴ M. Mochizuki and M. Imada, Phys. Rev. Lett. **91**, 167203 (2003).
¹⁵ T. Hahn (ed.), *International Tables for Crystallography, Vol. A: Space-Group Symmetries* (Dordrecht: Kluwer Academic Publishers, 1995).
¹⁶ The d orbitals given in Eq. (1) are normalized when integrated over the unit sphere. i.e., including the radial function $f(r)$, which obeys $\int f(r)r^2 dr = 1$, we have the following representations in real space:
 $\langle \mathbf{r} | xy \rangle = f(r) \times \sqrt{15/4\pi} xy/r^2$,
 $\langle \mathbf{r} | 2z^2 \rangle = f(r) \times \sqrt{5/16\pi} (2z^2 - x^2 - y^2)/r^2$,
 $\langle \mathbf{r} | yz \rangle = f(r) \times \sqrt{15/4\pi} yz/r^2$,
 $\langle \mathbf{r} | xz \rangle = f(r) \times \sqrt{15/4\pi} xz/r^2$,
 $\langle \mathbf{r} | x^2 - y^2 \rangle = f(r) \times \sqrt{15/16\pi} (x^2 - y^2)/r^2$.
¹⁷ S. A. Altshuler and B. M. Kozyrev, *Electron Paramagnetic Resonance in Compounds of Transition Elements* (London: Wiley, 1974).
¹⁸ K. I. Kugel and D. I. Khomskii, JETP Sov. Phys. **37**, 725 (1973).
¹⁹ J. C. Slater, *Quantum Theory of Atomic Structure, Vol. II* (Amsterdam: McGraw-Hill, 1960).
²⁰ R. E. Watson, Phys. Rev. **118**, 1036 (1960).
²¹ T. Saitoh *et al.*, Phys. Rev. B **52**, 7934 (1995).
²² W. A. Harrison, *Electronic Structure and the Properties of Solids* (New York: Dover, 1989).
²³ R. M. Eremina *et al.*, cond-mat/0407264 (2004).
²⁴ M. Takahashi, J. Phys. C **10**, 1289 (1977).
²⁵ L. Shekhtman *et al.*, Phys. Rev. Lett. **69**, 836 (1992).
²⁶ M. Cwik, private communication.
²⁷ C. Ulrich *et al.*, Phys. Rev. Lett. **89**, 167202 (2002).
²⁸ M. Braden, private communication.
²⁹ R. Schmitz, O. Entin-Wohlman, *et al.*, unpublished.
³⁰ M. N. Iliev *et al.*, Phys. Rev. B **69**, 172301 (2004).
³¹ L. Craco *et al.*, cond-mat/0309370 (2003).
³² B. Keimer, private communication.
³³ P. P. Ewald, Ann. Phys. Leipzig **64**, 253 (1921).
³⁴ J. M. Ziman, *Principles of the Theory of Solids* (Cambridge at the University Press, 1964).
³⁵ D. J. Newman, Adv. Phys. **20**, 179 (1971).